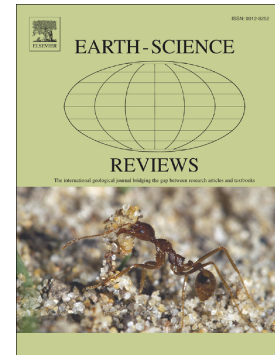# Accepted Manuscript

Age of the Barremian–Aptian boundary and onset of the Cretaceous Normal Superchron

Hugo K.H. Olierook, Fred Jourdan, Renaud E. Merle

Please cite this article as: H.K.H. Olierook, F. Jourdan and R.E. Merle, Age of the Barremian–Aptian boundary and onset of the Cretaceous Normal Superchron, Earth-Science Reviews, https://doi.org/10.1016/j.earscirev.2019.102906

Age of the Barremian–Aptian boundary and onset of the Cretaceous Normal Superchron

Hugo K.H. Olierook[1,2,3,*] hugo.olierook@curtin.edu.au, Fred Jourdan[1,4], Renaud E. Merle[5]

[1] School of Earth and Planetary Sciences, Curtin University, GPO Box U1987, Perth, WA 6845, Australia

[2] Centre of Exploration Targeting – Curtin Node, Curtin University, GPO Box U1987, Perth, WA 6845, Australia

[3] John de Laeter Centre, Curtin University, GPO Box U1987, Perth, WA 6845, Australia

[4] Western Australian Argon Isotope Facility & JdL Centre, Curtin University, GPO Box U1987, Perth, WA 6845, Australia

[5] Swedish Museum of Natural History, S-104 05 Stockholm, Sweden

[*] Corresponding author.

ABSTRACT

The age assigned to the boundary of the Barremian and Aptian stages remains one of the most poorly constrained post-Pangean stratigraphic boundaries. The lack of a Global Boundary Stratotype Section and Point (GSSP) for the stage boundary has hampered efforts to calibrate the absolute age of the Cretaceous period in the geological time scale. The Barremian–Aptian boundary also approximates the onset of magnetic polarity chron M0r; the end of this chron denotes the start of the Cretaceous Normal polarity Superchron that is of fundamental importance for plate reconstructions. Currently, there is up to 5% discrepancy in the age estimates of the Barremian–Aptian boundary (ca. 126–121 Ma) and the start of the Cretaceous Normal Superchron. Here, we review available geochronological information from the late Barremian and early Aptian stages collected from the Pacific Ocean, China, California, the Ontong Java Nui large igneous province and the High Arctic large igneous province. By utilizing only robust geochronological data including U-Pb and recalibrated $^{40}Ar/^{39}Ar$ ages from sites with magnetic polarity information and/or paleontological constraints, we calculate a best estimate of between 123.8 and 121.8 Ma for the Barremian–Aptian boundary and the onset of chron M0r at 2σ confidence. Using estimates of the duration of chron M0r (0.49 ± 0.10 Myr, 2σ), we conservatively compute the start of the Cretaceous Normal Superchron to between 123.4 and 121.2 Ma (2σ). Using an age of 83.07 ± 0.15 Ma (2σ) for the end of the Cretaceous Normal Superchron, the duration of the superchron is also constrained to between 38.0 and 40.5 Myr (2σ). These age ranges for the Barremian–Aptian boundary, the onset of the Cretaceous Normal Superchron and the duration of the superchron currently provide the best estimates until a GSSP is formally ratified.

Keywords: Chron M0r; Chron C34; Cretaceous Quiet Zone; $^{40}Ar/^{39}Ar$ geochronology; GSSP; Geological time scale

1   INTRODUCTION

The age of the Barremian–Aptian chronostratigraphic stage boundary remains one of the most poorly constrained stratigraphic boundaries since the breakup of Pangea (Cohen et al., 2013). The Barremian–Aptian stage boundary is somewhat unusual in that it is only just above the base of the reversely-polarized magnetic chron M0r (Frau et al., 2018), which immediately predates the Cretaceous Normal Superchron. Despite numerous proposals (Channell et al., 2000; Erba et al., 1996), the lack of a Global Boundary Stratotype Section and Point (GSSP) has significantly hampered efforts to pinpoint the stage boundary (e.g., Frau et al., 2018). However, even without a GSSP, the range of proposed ages that is currently used is abnormally large for any post-Pangean stage boundary (i.e., post-Triassic). The International Commission on Stratigraphy has currently placed the Barremian–Aptian boundary in the geological time scale (v2018/8) at ~125 Ma (Cohen et al., 2013). However, previous studies have placed the Barremian–Aptian Boundary (chron M0r; Channell et al., 1995) at 113.7 Ma (Fiet et al., 2006), 121.0 ± 1.4 (Gradstein et al., 1994; Opdyke and Channell, 1996), 121.2 ± 0.5 Ma (He et al., 2008), 121.5 ± 1.0 (Malinverno et al., 2012), ~121–122 Ma (Midtkandal et al., 2016), 124.6 ± 0.3 Ma (Ogg and Smith, 2004) or 126.3 ± 0.4 Ma (all uncertainties are at 2σ; Gradstein et al., 2012; Ogg, 2012). With the exception of the ca. 114 Ma age from Fiet et al. (2006), all these proposed ages for the chronostratigraphic boundary are still used in studies for various applications at the present day (Erba et al., 2015; Huang, 2018; Müller et al., 2016; Young et al., 2018), leaving investigators with a range of options based on individual preferences. The wide variation in the age of the Barremian–Aptian boundary is mainly due to a lack of direct drill hole age constraints on both the seafloor and on land, and variable interpretation of previous geochronological, magnetic, paleontological and cyclostratigraphic data.

Establishing a more accurate numerical age for the Barremian–Aptian boundary – and the base of chron M0r – is of fundamental importance for several applications in the geosciences. First, linking the biostratigraphic and magnetostratigraphic record with numerical ages provides a reference for correlating the fossil record and magnetic reversals across the world (e.g., Karpuk et al., 2018). Although this is generally important for all stage boundaries that lack a GSSP, the Barremian–Aptian boundary remains one of the most poorly constrained stage boundaries after the breakup of Pangea. Second, the early Aptian is associated with major climatic and biotic crises. It records oceanic anoxia event 1a (OAE1a), a major crisis in Cretaceous oceanography (e.g., Erba, 2004; Erba et al., 2015; Leckie et al., 2002; Midtkandal et al., 2016) and is associated with a greenhouse pulse (Larson and Erba, 1999) before long-term hothouse conditions in the Late Cretaceous were established (Forster et al., 2007; Jenkyns, 2010; Jenkyns et al., 2002). Thus, understanding intrinsic and extrinsic causes for these major crises requires an accurate absolute age for the Barremian–Aptian boundary. Third, the Early Cretaceous is associated with emplacement of multiple large igneous provinces, including the two largest in the Phanerozoic – Kerguelen (Coffin et al., 2002; Frey et al., 2000; Olierook et al., 2019c; Olierook et al., 2017; Olierook et al., 2015) and Ontong Java Nui (Hoernle et al., 2010; Larson and Olson, 1991; Neal et al., 2008; Taylor, 2006; Tejada et al., 2002; Timm et al., 2011). The emplacement of several large igneous provinces in a relatively short temporal window have often been attributed to mantle plume production from slab graveyards caused from circum-Pangean subduction zones (Burke et al., 2008; Kendall and Silver, 1996; Steinberger, 2000). A lack of accurate ages hampers linking plume–plate processes and magmatic–biotic processes (Santosh, 2010). Fourth, the Barremian–Aptian boundary also corresponds to the start of reversely-polarized chron M0r. The end of chron M0r denotes the start of normally-polarized chron C34 – the Cretaceous Normal Superchron or Cretaceous Quiet Zone – the longest period of no

significant magnetic reversals since the breakup of Pangea (Granot et al., 2012; Helsley and Steiner, 1968; Larson and Olson, 1991). Lasting ~40 Myr from ~125–120 Ma to ~83 Ma, the ages at which the Cretaceous Normal Superchron starts (chron M0y) and ceases (chron C34y) are of paramount importance for yielding accurate plate reconstructions. Fifth, the age range of the Cretaceous Normal Superchron also comprises one of only two global plate reorganization events (Matthews et al., 2012; Müller et al., 2016). Understanding how plate velocities have varied during plate reorganizations and whether these impacted the climatic or biotic record requires accurate ages for the onset and end of the Cretaceous Normal Superchron. With the current uncertainty in onset age of the Cretaceous Normal Superchron (~125–120 Ma), current plate reconstructions have an additional uncertainty of ~14% on spreading velocities during this time. Lastly, links have also been proposed between the Earth's dynamo, activities in the lower mantle and superchrons (Glatzmaier et al., 1999; Jacobs, 2001; Larson and Olson, 1991; Olson et al., 2012). Whether superchrons are related to external consequences such as the impingement of a subducted slab with the core–mantle boundary (Courtillot and Olson, 2007; Larson and Olson, 1991) or whether these are intrinsic to the Earth's magnetic field as predicted by dynamo theory (Hide, 2000; Olson et al., 2012) requires accurate age constraint to test theories. Therefore, accurate and more precise ages for the Barremian–Aptian boundary and onset of the Cretaceous Normal Superchron are paramount in order to begin to understand the drivers for all these applications.

In this contribution, we review all available geochronological data in combination with stratigraphic sections for sites that have reliable paleontological and/or magnetostratigraphic constraints (Fig. 1). Using strict criteria (see below), the age of the both the Barremian–Aptian boundary and, subsequently, the onset of the Cretaceous Normal Superchron is constrained to a 2.0 and 2.2 Myr window at 2σ uncertainty, respectively.

Ultimately, these refined ages and their uncertainties provide a better numerical estimates that can be used for testing fundamental questions in the Earth sciences.

2   ASSESSMENT CRITERIA FOR AGE DATA

In order to constrain the Barremian–Aptian boundary, studies have used a variety of geochronological and other numerical dating techniques including U-Pb (Midtkandal et al., 2016), $^{40}Ar/^{39}Ar$ (He et al., 2008), K-Ar (Armstrong, 1978), Rb-Sr (Armstrong, 1978) and cyclostratigraphic techniques (Huang et al., 2010). These different techniques have their benefits and limitations, and these limitations need to be assessed for robustness. For all geochronological data, multiple data points from the same sample should not be able to reject the null hypothesis such that a weighted mean of individual analyses should have a probability of ≥0.05 (Baksi, 2006; York, 1966; York, 1969). This first order requirement necessitates that multiple grains, plateau steps or aliquots are analyzed to yield a statistically-valid weighted mean age for a single sample.

For U-Pb data, it is important that only data that are concordant are used (i.e., $^{206}Pb/^{238}U$ and $^{207}Pb/^{235}U$ dates overlap with the concordia curve at 2σ). Chemical abrasion prior to isotope dilution thermal ionization mass spectrometry (CA-ID-TIMS; Mattinson, 2005) can aid in reducing discordance such that all robust analyses should be concordant. Here, zircon is the preferred mineral because it is a ubiquitous trace mineral in felsic and, to a lesser extent, intermediate and mafic rocks (Corfu et al., 2003; Speer, 1980). Its success in geochronology stems from its physical and chemical properties, including its relative durability hardness (Mohs scale = 7.5), chemical inertness, incorporation of trace amounts of U and Th during crystallization (Bea, 1996), rejection of Pb incorporation during crystallization (i.e., negligible common-Pb; Harley and Kelly, 2007; Watson et al., 1997) and extreme closure temperature to Pb (>900 °C; Cherniak and Watson, 2001; Lee et al., 1997).

Other U-bearing and common-Pb resistant minerals such as monazite and baddeleyite are also useful geochronometers but are less commonly employed (Piechocka et al., 2017; Wingate and Giddings, 2000). Minerals such as titanite or apatite that usually incorporate significant quantities of common-Pb can be less robust than common-Pb resistant minerals due to the lack of concordance (Kirkland et al., 2017; Olierook et al., 2019a; Olierook et al., 2019d). In situ U-Pb techniques such as laser ablation inductively-coupled plasma mass spectrometry (LA-ICP-MS) or secondary ion mass spectrometry (SIMS) are also effective techniques of obtaining reliable U-Pb ages (e.g., Olierook et al., 2019b; Olierook et al., 2018; Spencer et al., 2016) but these do not have the resolution of TIMS data (<0.5% uncertainty at 2σ). Nevertheless, in situ techniques can still yield robust ages and any acquired data are considered in this review.

For $^{40}Ar/^{39}Ar$ data, only step-heated data is considered as total fusion analyses lack multiple analyses necessary to test the null hypothesis (Baksi, 2006). At least 50% (preferably 70%) of all ^{39}Ar released should be distributed over a minimum of three consecutive steps agreeing at 2σ (Baksi, 2007). Furthermore, age data need to be recalculated to ^{40}K decay constants and standards that have been calibrated against U-Pb data. We utilize the model of Renne et al. (2010), updated in Renne et al. (2011), which is favoured over Kuiper et al. (2008) because the former study is the only one that directly calibrates U-Pb ages with robust $^{40}Ar/^{39}Ar$ ages. Moreover, the study of Kuiper et al. (2008) does not explicitly recommend new ^{40}K decay constants but rather used the decay constants proposed by Min et al. (2000), which was a preliminary version of Renne et al. (2010) and Renne et al. (2011). The material that was analyzed for $^{40}Ar/^{39}Ar$ geochronology is also critiqued. Groundmass and whole-rock data can have cryptic alteration that cannot be visually assessed during hand-picking, whereas mineral separates (particularly colorless minerals like plagioclase) circumvent many of the alteration issues (Baksi, 2007; Hofmann et al., 2000;

Merle et al., 2009; Verati and Jourdan, 2014). Therefore, mineral separates are preferred as any alteration in groundmass or whole-rock may produce younger ages that record (hydrothermal) alteration rather than crystallization (Merle et al., 2018; Merle et al., 2019).

Rb–Sr and K–Ar data both have significant limitations that prevents them from being useful for the more accurate and precise determination of the Barremian–Aptian boundary. Rb–Sr data can be effective from a single sample if multiple minerals (e.g., biotite, muscovite, K–feldspar) yield a statistically-reliable isochron (Davidson et al., 2005). However, as a robust and precise ages requires multiple minerals to yield sufficient spread in the isochron, there are usually not more than three or four data clusters that allow for an age calculation (Davidson et al., 2005). K–Ar is equally problematic because it cannot unambiguously demonstrate that a sample is free of alteration nor contains excess or inherited ^{40}Ar (Kelley, 2002; Verati and Jourdan, 2014). Moreover, the step-heating approach of ^{40}Ar/^{39}Ar yields multiple plateau steps that can be rigorously assessed for statistical robust via the null hypothesis. Most studies rarely report more than two analyses from the same sample, so that the null hypothesis cannot be adequately tested (McDougall et al., 1999). Finally, K–Ar also requires that any sample is split into two, with one part analyzed for K and the other for Ar, and sample equivalence cannot be conclusively demonstrated. On the basis of these technique limitations, Rb–Sr and K–Ar data are not used to constrain the age of the Barremian–Aptian boundary.

Orbitally-tuned cyclostratigraphic constraints are useful for short time intervals as they are usually more precise than geochronological constraints (Huang, 2018). Moreover, sedimentary sections to which cyclostratigraphic principles can be applied to are more common than horizons that can be dated via U-Pb (e.g., ash falls) or ^{40}Ar/^{39}Ar (basaltic lava flows). Astronomically-constrained ~405 Kyr orbital eccentricity cycles tend to be the most robust of cyclostratigraphic constraints, and have been shown to be reliable as far back as the

Triassic (Kent et al., 2018). However, the interpretation of cyclostratigraphic data is not always straightforward. Across particularly large gaps without geochronological constraints, over- or under-identification of eccentricity cycles can lead to significant errors.

For all geochronological data, all uncertainties quoted in this paper are at 2σ and include all sources of error [including decay constants in square brackets] unless otherwise noted.

3   BRIEF HISTORICAL ACCOUNT OF THE NUMERICAL AGE FOR THE BARREMIAN–APTIAN BOUNDARY

The assignment of the Barremian–Aptian boundary is an ongoing process (Ogg et al., 2012). The Aptian sequence was originally named after the village of Apt in the Vaucluse province of southeastern France (Orbigny, 1840). The majority of work leading up to the mid-1990s focussed primarily on biostratigraphic correlations of ammonites (cf. review by Moullade et al., 2011). The French Aptian sections are relatively poor in ammonites and, consequently, the classical marker for the base of the Aptian was the lowest occurrence of the deshayesitid ammonite *Prodeshayesites* in northwestern Europe (Hoedemaker et al., 2003; Moullade et al., 1998a; Moullade et al., 1998b; Rawson, 1983). However, the earliest Aptian is also associated with a major transgression so that virtually no ammonoid-bearing section spans across the Barremian–Aptian boundary. Based on revisions of all available biostratigraphic data – and coupled with a host of other physical stratigraphic data – Erba et al. (1996) proposed that the base of chron M0r should be utilized as the base of the Aptian. Although acknowledging that the ammonite biostratigraphic and magnetostratigraphic are not exactly equivalent with the base of chron M0r situated within the uppermost Barremian (Frau et al., 2018; Wissler et al., 2002), this discrepancy is far smaller than the current uncertainty on the numerical age of the Barremian–Aptian boundary. An alternative concept was

proposed by Moullade et al. (2011) to use the base of the *Dufrenoyia furcata* ammonite zone but this was swiftly rejected by the Lower Cretaceous ammonite working group (Reboulet et al., 2011). Thus, the use of the base of chron M0r still represents the best approximation for the Barremian–Aptian boundary.

The first major effort in using geochronological data (K–Ar, Rb–Sr and U-Pb ages) to calibrate the Barremian–Aptian boundary, amongst other stages, was done by Armstrong (1978). However, the use of many of these radiometric ages would fail modern statistical and other reliability criteria (see section 2). Continued calibration in the 1980s and early 1990s of the Barremian–Aptian boundary in the context of Mesozoic time scales similarly relied on often dubious geochronological data when assessed by modern standards (Cowie and Bassett, 1989; Haq et al., 1987; Harland et al., 1990; Odin, 1990; Palmer, 1983). In the mid-1990s, whole-rock $^{40}Ar/^{39}Ar$ data from ODP drilling MIT Guyot in the western Pacific (Pringle and Duncan, 1995; Pringle et al., 1994), whole-rock $^{40}Ar/^{39}Ar$ data from the Ontong Java Plateau (Mahoney et al., 1993) and zircon U-Pb data reported in a conference abstract from the Great Valley Group in California (Coleman and Bralower, 1993) led several workers to refine the Barremian–Aptian boundary to 121.0 ± 1.4 Ma (Channell et al., 1995; Gradstein et al., 1994; Opdyke and Channell, 1996). Each of these sites is discussed in more detail in the ensuing sections in this paper. This age of ca. 121 Ma for the Barremian–Aptian boundary, 're-affirmed' by Gee and Kent (2007) on the basis of magnetostratigraphy, is still favoured in many plate reconstructions (Müller et al., 2016; Seton et al., 2012; Young et al., 2018) over more recent revisions to the age of the Barremian-Aptian boundary. Older ages (e.g. ≥125 Ma) for M0r result in lower seafloor spreading rates in the mid-Cretaceous and diminish temporal correlations between pulses of seafloor production (fast spreading rates) and sea level high-stands (Seton et al., 2009).

In the 2000s and 2010s, the age of the Barremian–Aptian boundary adopted in the geological timescale became progressively older. The jump in age from 121.0 ± 1.4 in the 1990s (Channell et al., 1995; Gradstein et al., 1994; Opdyke and Channell, 1996) to 124.6 ± 0.3 Ma in the 2000s (Ogg and Smith, 2004; Pringle et al., 2003) in the geological time scale is primarily a result of the treatment of age data and interpretation of magnetic and biostratigraphy from the MIT Guyot in the western Pacific Ocean (see section 3.1 and Pringle et al., 2003).

Further updates of the geological time scale in 2012 pushed back the age of the Barremian–Aptian boundary to ca. 126.3 Ma (Ogg, 2012; Ogg et al., 2012) principally on the basis of cyclostratigraphy (Huang et al., 2010), with additional geochronological data (discussed in subsequent section) and recalibration of $^{40}Ar/^{39}Ar$ ages to U-Pb calibrated ^{40}K decay constants (Renne et al., 2011; Renne et al., 2010). The principal issue here is the use of cyclostratigraphy. The Aptian cyclostratigraphy in Huang et al. (2010) is tied only to the Albian–Cenomian boundary at 100.62 Ma without further radiometric age ties. Across particularly large gaps such as the gap between the base Aptian and base Cenomanian, over- or under-identification of eccentricity cycles (>60 in Huang et al., 2010) can lead to significant errors. The use of a significantly older Barremian–Aptian boundary of ca. 126.3 Ma leads to problems further back in the Early Cretaceous (Aguirre-Urreta et al., 2015; Ogg et al., 2016b; Vennari et al., 2014), which suggest that the geological time scale may need to be shifted "~2 Myr younger" (Huang, 2018). Clearly, there is a strong need to revisit the available radioisotopic data in light of these geological time scale issues.

Currently, the Barremian–Aptian boundary is ca. 125 Ma in the geological time scale (Cohen et al., 2013). This age is is in between what was used in the 2004 (Gradstein et al., 2004), and the 2012 and 2016 geological time scales (Gradstein et al., 2012; Ogg et al., 2016a). However, the rationale for this age is not clearly justified. Ultimately, the lack of a

consensus in the scientific community calls for a reassessment of the geochronological data in the context of magnetostratigraphy, biostratigraphy and cyclostratigraphy to assess whether a refinement of the Barremian–Aptian boundary is possible.

4   SITES WITH AGES FOR THE BARREMIAN–APTIAN BOUNDARY AND CHRON M0R

4.1   *MIT Guyot, western Pacific Ocean*

Drilling of the MIT Guyot during Ocean Drilling Program Leg 144 at site 878 in 1993 revealed three separate volcanic episodes with different whole-rock major and trace element, and Sr–Nd–Pb isotopic compositions, separated by weathering horizons (Fig. 2b; Koppers et al., 1995; Koppers et al., 1998). Pringle and Duncan (1995) reported whole-rock $^{40}Ar/^{39}Ar$ isochron weighted mean ages of 122.9 ± 1.8 Ma ($n = 3$ of 3 samples), 121.7 ± 3.2 Ma ($n = 1$ of 1 sample) and 119.6 ± 1.4 Ma ($n = 3$ of 3 samples) for the lower alkali basalt, middle basanite and upper trachybasalt lava flows, respectively (Fig. 2b).

The lower alkali basalt flow is situated on the magnetic transition between a reversely- and normally-polarized chron, whereas the middle basanite and upper trachybasalt flows reside exclusively within a normally-polarized chron (Fig. 2b; Gee and Nakanishi, 1995). These were originally interpreted to represent chron M1r and M1n (Pringle and Duncan, 1995). Pringle et al. (2003) question whether the reversely- and normally-polarized chrons may instead be M0r to C34n (i.e., the Cretaceous Normal Superchron). This interpretation, together with new cyclostratigraphic interpretations of Huang et al. (2010), was a major factor in revising the ages to ~124.6 Ma (Ogg and Smith, 2004) and 126.3 Ma (Ogg, 2012) for the Barremian–Aptian boundary. The primary basis for choosing M0r and C34n is a suggestion that the Aptian nannoconid crisis (Erba, 1994; Erba, 2004; Larson and

Erba, 1999) may not have been present in the western Pacific Ocean (Pringle et al., 2003). However, there is now strong evidence that the nannoconid crisis did occur in the western Pacific, potentially triggered by the eruption of the Ontong Java Nui large igneous province (Erba et al., 2015 and references therein). Given the close spatial association of the Ontong Java Nui large igneous province and the MIT Guyot (Fig. 1), it would be very unlikely that the nannoconid crisis is not recorded at the MIT Guyot. Pringle et al. (2003) also offer an alternative explanation, that the originally-reported age for the upper lava flows (119.6 ± 1.4 Ma) is too young because cryptic alteration cannot be visually detected with whole-rock (or groundmass) samples. Whole-rock (or groundmass) ages could be up to 10% younger than their equivalent mineral separates in samples that yield statistically-valid $^{40}Ar/^{39}Ar$ plateaus (Baksi, 2007; Hofmann et al., 2000; Merle et al., 2018). Even if whole-rock alteration did not affect MIT Guyot samples, at the very least the original ages reported by Pringle and Duncan (1995) were calculated using the now outdated ^{40}K decay constants of Steiger and Jäger (1977). The ^{40}K decay constants have since been revised in 2000 (Min et al., 2000) and again in 2010 (Renne et al., 2011; Renne et al., 2010), which makes all previous $^{40}Ar/^{39}Ar$ ages older by ~1%. In addition, using up-to-date standard intercalibration values (F-values; Jourdan and Renne, 2007; Renne et al., 1998) can also commonly increase a given age by a further 1–2 %, depending on the original reference standard. By recalculation of the ages to the correct decay constants and standard ages, we show below that the earlier interpretation of the M1n and M1r magnetic polarity zones drilled in the MIT Guyot is more plausible with the magneto- and biostratigraphic record (Gee and Nakanishi, 1995; Pringle and Duncan, 1995).

To compute the correct age closest to Barremian–Aptian boundary at the MIT Guyot, we use only samples from the upper flow (i.e., assumed to be closest to the Barremian–Aptian boundary, chron M0r) and those that yielded plateaus at 2σ confidence (i.e., >70% of

total ^{39}Ar released) with a p value >0.05 and are defined by more than three consecutive heating steps. Mini-plateaus (i.e., between 50 and 70% of the total ^{39}Ar released) are considered only if they support an existing plateau age which is indistinguishable within uncertainties. Pringle and Duncan (1995) reported two plateau ages, recalculated at 121.1 ± 1.4 Ma (91% of ^{39}Ar released; recalculated MSWD = 0.11, p = 0.95) and 119.9 ± 2.6 Ma (71% of ^{39}Ar released; recalculated MSWD = 1.2, p = 0.31) that satisfy these criteria, supported by a mini-plateau age of 119.9 ± 1.6 Ma (59% of ^{39}Ar released; recalculated MSWD = 0.59, p = 0.67). Note, as Pringle and Duncan (1995) only presented their ^{40}Ar/^{39}Ar data in graphical form and did not report MSWD or p values, we have calculated these from redrawing and recomputing their figures and so the MSWD and p values may be slightly in error. There is no evidence for excess argon, with all measured ^{40}Ar/^{36}Ar ratios (335 ± 90, 379 ± 139 and 295 ± 52, respectively) overlapping within 2σ error of the atmospheric ^{40}Ar/^{36}Ar ratio of 298.56 ± 0.31 (Lee et al., 2006). Using these three individual ages, we calculate a weighted mean age of 123.5 ± 1.0 [1.3] Ma (MSWD = 0.89, p = 0.41, Table 1, Fig. 2c). Note that the uncertainty might be slightly underestimated if the three aliquots have the same J-values in their calculation as this would potentially create small correlated uncertainties (cf. discussion in Jourdan et al., 2007). As these samples were probably from chron M1n (Gee and Nakanishi, 1995; Pringle and Duncan, 1995), this age represents a strict maximum age as this unit as it is below the Barremian–Aptian boundary. Alternatively, if this sample is from chron C34n (Pringle et al., 2003), then this age is a strict minimum age.

Summary. *Limitations*: Whole-rock analyses, uncertain magnetostratigraphy, graphical form data only in Pringle and Duncan (1995). *Best age estimate*: 123.5 ± 1.0 [1.3] Ma for chron M1r (uppermost Barremian).

4.2   *Liaoning Province, China*

Several radioisotopic age data are available for the Liaoning Province in China from the upper Barremian and lower Aptian sequences (Fig. 3a,b). Geochronological constraints from the Yixian Formation, the conformably-overlying Jiufotang Formation and unconformably underlying Tuchengzi Formation constrain the age of the Yixian Formation to ca. 131−122 Ma (Fig. 3b). There are some discrepancies in age data with respect to the stratigraphic succession of the Yixian Formation, particularly with respect to some of the ages recalculated from Chang et al. (2009), which tend to be slightly older than ages from all other studies (Fig. 3b). Another obstacle that the Yixian Formation presents is that its biostratigraphy is not well tied to global correlations (Wang et al., 2016b), so that biostratigraphically pinpointing the Barremian−Aptian boundary is difficult within the Yixian Formation (Fig. 3b).

As an alternative to biostratigraphic constraints, two sites in the Liaoning Province have been dated within reversely-polarized horizons that may correspond to chron M0r (He et al., 2008; Zhu et al., 2004). The first site is situated within the lower to middle Yixian Formation, specifically at the Mashenmiao−Zhuanchengzi section (He et al., 2008). Although the study does not report the exact stratigraphic location, petrographic and geochronological data imply that the andesitic sample was probably from the Upper Lava Unit (Fig. 3b). Three groundmass ^{40}Ar/^{39}Ar apparent ages from lava flows within the Yixian Formation were reported from which only one of these ages yielded a reliable plateau age of 121.7 ± 0.8 Ma (Table 1; He et al., 2008). This sample also yielded an ^{40}Ar/^{36}Ar intercept of 294.1 ± 5.3 that overlaps within 2σ error of the atmospheric ^{40}Ar/^{36}Ar ratio of 298.56 ± 0.31 (Lee et al., 2006), implying no evidence for excess argon. Age recalculation to the new decay constants of Renne et al. (2011) yields a corrected age of 122.9 ± 0.8 [1.1] Ma for the reversely-polarized sample in the Yixian Formation (Fig. 3c; He et al., 2008). Although mineral separates are preferred over groundmass, petrographic examination of thin sections here and

from other sites in the Yixian Formation suggest that geochemical alteration is minimal (Chang et al., 2017; Chang et al., 2009; He et al., 2008).

The authors argue the ca. 123 Ma sample is situated within chron M0r on the basis of its age similarity to what was expected in the 2004 geological time scale (Ogg and Smith, 2004). Here, we consider whether this sample could have been situated in adjacent reversely-polarized chrons: the ISEA chron (M"-1r"; Zhu et al., 2004), the brief reverse polarity segment that occurred soon after the onset of the Cretaceous Normal Superchron (Tarduno, 1990), or chron M1r. Ages from the ISEA chron are highly uncertain and the current best estimate is from ODP site 879 (re-calculated to 121.4 ± 2.1 Ma; Pringle and Duncan, 1995), although we caution whether this unit was even dated within ISEA. Nevertheless, if the age of the ISEA chron is correct, then it is possible that He et al. (2008) dated an interval within the ISEA chron. If the sample originated instead from chron M1r, then the age of the Barremian–Aptian boundary would have to be at least ~2.3 Myr younger (i.e., duration of chron M1n from cyclostratigraphy; Fiet and Gorin, 2000) than 122.9 ± 0.8 (i.e., at least younger than ~120.6 Ma). Although the cyclostratigraphy may be slightly in error, the Barremian–Aptian boundary would be too young if He et al. (2008) dated a sample within chron M1r, even with the magnetostratigraphic time scales of Gee and Kent (2007). Furthermore, integration with other sites reveals that the interpretation of chron M0r for the Liaoning site is likely correct (see section 4). Thus, this age thus represents a minimum age for the Barremian–Aptian boundary and the onset of chron M0r.

The second reverse polarity site in the Liaoning Province is reported from a section near Jianguo but its exact stratigraphic position is uncertain (Zhu et al., 2004). The authors suspect that this is likely related to the ISEA chron on the basis of overlapping ages with the ISEA chron measured at. We recompute their reported age to an age of 120.0 ± 1.1 Ma (75% [39]Ar released, MSWD = 1.0, $p = 0.46$, 19 plateau steps, Table 2). There is no evidence for

excess argon based on the paucity of trapped Ar. Although this age overlaps within 2σ of the supposed ISEA chron measured at ODP 879, it also overlaps with the Gee and Kent (2007) magnetostratigraphic time scale. As with the other sample, integration with other ages from other global localities is key (see section 4). As an age of 120.0 ± 1.1 Ma also falls outside the uncertainty of the other reported sites either above or below the Aptian–Barremian boundary, we concur with the original authors' interpretation that this age belongs to the ISEA and we suggest that this sample is probably situated in the Jiufotang Formation. It is worth noting that two other reverse chrons in the Cretaceous Normal Superchron (M"-2r" ≈ 108 Ma; M"-3r" ≈ 102 Ma) occurred significantly later (Ogg and Smith, 2004) than measured in the Liaoning Province (Zhu et al., 2004).

Summary. *Limitations*: Groundmass analyses, uncertain biostratigraphy. *Best age estimate*: 122.9 ± 0.8 [1.1] Ma for chron M0r (lowermost Aptian).

4.3   *California, USA*

The Great Valley Group in California records a Lower Cretaceous sequence with well-characterized calcareous nannofossil zonation (Fig. 4a, b; Bralower, 1990; Bralower et al., 1995). Part of the Valanginian to Aptian sequence has intercalated ash fall (bentonite) horizons that have been dated via zircon U-Pb TIMS but are only available from an abstract (Coleman and Bralower, 1993) and from a Masters thesis (Shimokawa, 2010). Although the abstract does not have the raw data and its validity cannot be verified, the study by Shimokawa (2010) has all the raw data. Nevertheless, we treat this unpublished data with caution when assessing it collectively with other sites.

One bentonite sample taken from a lower Aptian succession yielded seven concordant CA-ID-TIMS dates that spread from ca. 127 to 124 Ma (Fig. 4c). The youngest four analyses cluster, yielding a weighted mean $^{206}Pb/^{238}U$ age of 124.08 ± 0.15 [0.23] Ma (MSWD = 1.7, *p*

= 0.16, Fig. 4c). The other, older three analyses are probably antecrystic or xenocrystic (Fig. 4c). This sample was taken from the *Chiastozygus litterarius* biozone (NC6A subzone, Fig. 4b; Bralower et al., 1995). A paleontological sample collected directly below the bentonite layer yielded the first occurrence of *C. litterarius* and last occurrence of *Conusphaera rothii* (i.e., NC6A subzone; Bralower, 1990). Although these calcareous nannofossils were original interpreted as earliest Aptian (Bralower, 1990; Bralower et al., 1995), revisions have shown that *C. litterarius* is also present in the uppermost Barremian (Bown et al., 1998). Thus, the ash fall may have been deposited in the uppermost Barremian or lowermost Aptian (Shimokawa, 2010).

Summary. *Limitations*: Unpublished analyses, no magnetostratigraphy. *Best age estimate*: 124.08 ± 0.15 [0.23] Ma for uppermost Barremian or lowermost Aptian.

4.4 *Greater Ontong Java Event, southwestern Pacific Ocean*

The Ontong Java Nui large igneous province, or Greater Ontong Java large igneous province, comprises the once-contiguous Ontong Java, Manihiki and Hikurangi oceanic plateaus (Taylor, 2006). The earliest portions are known as the Greater Ontong Java Event. The age of the Greater Ontong Java Event is fundamentally important for the Barremian–Aptian boundary because it is purported to post-date the Barremian–Aptian boundary and may have been the cause of OAE1a (Erba et al., 2015). We detail the available age data of all three oceanic plateaus here.

4.4.1 *Ontong Java Plateau*

The Ontong Java Plateau erupted solely below sea level but obducted sections now outcrop in the northeastern Solomon Islands (Fig. 5a; Tejada et al., 2002). On the offshore portion of the Ontong Java Plateau, the Greater Ontong Java Event is recorded at DSDP site 289, and ODP sites 807 and 1184 (Chambers et al., 2004; Mahoney et al., 1993).

From DSDP site 289 and ODP site 807, all ages were obtained via whole-rock $^{40}Ar/^{39}Ar$ geochronology and were supported by magneto- and biostratigraphy (Fig. 5b–c). Two samples from the same lava flow in DSDP Site 289 yielded re-calculated ages of 125.8 ± 4.9 and 124.6 ± 5.5 Ma, with a weighted mean of 125.3 ± 3.6 Ma (MSWD = 0.11, p = 0.74; Mahoney et al., 1993). Six samples from DSDP Site 807 yielded recalculated ages between 127.7 ± 4.5 Ma and 122.8 ± 5.3 Ma (Mahoney et al., 1993). These ages represent different lava flows emplaced at different times but because of the unusually low-precision of these analyses, all their apparent ages overlap at 2σ. Samples dated from ODP site 807 (Mahoney et al., 1993) are directly overlain by sedimentary rocks containing Aptian planktonic foraminifera (Sliter and Leckie, 1993) and Aptian calcareous nannofossils (Channell et al., 1995). For the nannofossils, the first occurrence of *Rucinolithus irregularis*, the absence of *Eprolithus floralis* and the scarcity of nannoconids indicates that the overlying sedimentary rocks can be attributed to the upper part of C. *litterarius* zone, above the nannoconid crisis and thus occurring after the onset of the Cretaceous Normal Superchron (Channell et al., 1995). The nannofossil interpretation is supported by paleomagnetic direction results that demonstrate that all samples were collected from normally-polarized units, and that these probably correspond to the Cretaceous Normal Superchron (Musgrave et al., 1993; Tarduno et al., 1991).

From ODP site 1184, four small population plagioclase separates – with two aliquots of 4–5 crystals each – from basaltic clasts were dated by $^{40}Ar/^{39}Ar$ total fusion (Table 4; Chambers et al., 2004). Total fusion may hide the effects of excess argon or alteration, such that the age may be incorrect and contain unresolved yet systematic bias, giving the illusion that the age is correct. For example, only two samples yielded dates where both aliquots overlapped at 2σ (Chambers et al., 2004); the other two samples have probably suffered from excess argon or alteration. Moreover, the samples from ODP site 1184 were entrained in

Eocene sedimentary rocks (Sikora and Bergen, 2004), preventing detailed bio- or magnetostratigraphic constraints. Therefore, the reported ages from ODP site 1184 are not considered.

Outcropping portions of the Ontong Java Plateau have been dated on Malaita, Santa Isabel and Ramos Island (Solomon Islands) but these have virtually no sedimentary intercalations so that biostratigraphic constraints are difficult to assess (Tejada et al., 1996; Tejada et al., 2002). From Malaita Island, recalculated Early Cretaceous whole-rock ^{40}Ar/^{39}Ar plateau and mini-plateau ages ranged between 129.1 ± 3.9 Ma and 124.7 ± 3.3 Ma (Table 4; Mahoney et al., 1993; Tejada et al., 1996; Tejada et al., 2002). One Early Cretaceous whole-rock ^{40}Ar/^{39}Ar plateau age was reported from Santa Isabel Island at 126.3 ± 3.1 Ma (100% ^{39}Ar released, 4 steps) and another sample from Ramos Island, just north of Santa Isabel, at 123.0 ± 3.3 Ma (100% ^{39}Ar released, 4 steps; Tejada et al., 1996). It is worth noting that that all samples from the Solomon Islands were calculated relative to FCT-3 biotite, which shows chemical heterogeneity and poor single grain ^{40}Ar*/^{40}K reproducibility (Dazé et al., 2003). Utilization of an unreliable standard might yield a poor flux monitoring and slightly bias the resulting ^{40}Ar/^{39}Ar ages of investigated samples. However, use a 10 mg-aliquot of FCT-3 standard (as used at least in Tejada et al., 2002) tends to homogenize the ^{40}Ar*/^{40}K to some extent (Duncan et al., 1997), so the FCT-3 biotite standard may be acceptable. For all Solomon Island samples, no MSWD or p is available for the plateau ages, nor are ^{40}Ar/^{39}Ar spectra available to assess their validity. An additional problem is that whole-rock was used as opposed to mineral separates. Whole-rock and, to a lesser extent, groundmass may contain alteration that can be visually undetectable because of the opaque nature of whole-rock and groundmass during picking under a binocular microscope.

4.4.2 *Manihiki Plateau*

The early portions of Manihiki Plateau erupted solely in the submarine domain (Timm et al., 2011). Eleven robust $^{40}Ar/^{39}Ar$ ages have been obtained from the Manihiki Plateau from one location in the centre of the High Plateau (DSDP site 317) and several dredging expedition around the scarp margins of the High and Western Plateaus (Fig. 5a; Hoernle et al., 2010; Ingle et al., 2007; Timm et al., 2011). The most important sampling site is that of DSDP site 317 because of auxiliary magneto- and biostratigraphic constraints (Fig. 5d). Two samples with two aliquots of plagioclase each yielded recalculated ages of 119.7 ± 3.8 and 119.4 ± 5.2 Ma from DSDP site 317 (Fig. 5d, Table 4; Hoernle et al., 2010). All paleomagnetic analyses older than the Campanian in DSDP site 317 are normally-polarized and all lava flows are therefore interpreted to have erupted during the Cretaceous Normal Superchron (Fig. 5d; Cockerham and Jarrard, 1976). Unfortunately, biostratigraphic constraints are not available beyond the upper Aptian (*Leupoldina cabri* planktonic foraminiferal zone, Fig. 5d) due to barren intervals to the bottom of DSDP site 317 (McNulty, 1976). Nevertheless, the magnetostratigraphic constraints indicate that the Barremian–Aptian boundary must be at the very least ~0.4–0.6 Myr older (i.e., the duration of chron M0r; Malinverno et al., 2010) than the ages recorded in both samples.

The dredges from the Manihiki Plateau are probably sampling closer to the basement than DSDP Site 317 (Fig. 5a). After recalculation to correct standard ages, the six oldest samples yielded plagioclase or glass $^{40}Ar/^{39}Ar$ ages between 128.4 ± 8.3 Ma and 125.9 ± 0.9 Ma (Table 4). One dredge sample from Ingle et al. (2007) with a reported age of 117.1 ± 3.5 Ma could not be recalculated because the standard used (EB-1 biotite) has not been properly intercalibrated (Table 4).

4.4.3 *Hikurangi Plateau*

The Hikurangi Plateau, located east of the North Island of New Zealand, is fully submarine with no outcrop available (Mortimer and Parkinson, 1996). The Greater Ontong

Java Event on the plateau remains poorly constrained despite recent dredging expedition (Hoernle et al., 2010). Single-crystal total fusion analyses of plagioclase feldspar yielded one robust age reported at 118.4 ± 4.0 Ma ($n = 16$ of 16 analyses, MSWD = 1.18, $p = 0.28$). However, the questionable analytical approach (cf. above for discussion about single crystal total fusion ages), the relatively high age uncertainty on only one sample and the lack of biostratigraphic and magnetostratigraphic constraints means that further work is needed to constrain the magmatic history of the Hikurangi Plateau.

4.4.4   *Barremian–Aptian boundary from the Greater Ontong Java Event*

With all the above considerations, the best age constraints for the Barremian–Aptian boundary from the Greater Ontong Java Event are those that have robust magneto- and/or biostratigraphic information, and are derived from >70% (^{39}Ar) plateau obtained by step-heating analyses, and these are only available from DSDP and ODP drill cores at the present day (Fig. 5b–d, Table 4). The Ontong Java Plateau yielded whole-rock ages of 125.3 ± 3.6 [3.9] Ma (DSDP 289) and 127.7 ± 4.5 [4.8] Ma to 122.8 ± 5.3 [5.6] Ma (ODP 807), and the Manihiki Plateau yielded two plagioclase ages of 119.7 ± 3.8 [4.1] Ma and 119.4 ± 5.2 [5.5] Ma (DSDP 317), all of which are from Aptian successions within the Cretaceous Normal Superchron. Considering that chron M0r lasted 0.49 ± 0.10 Myr (Malinverno et al., 2010), the Barremian–Aptian boundary must be at least 0.39 Myr older than the ages recorded at DSDP 289, ODP 807 and DSDP 317. This equates to 125.7 ± 3.6 [3.9] (DSDP 289), 128.1 ± 4.5 [4.8] Ma to 123.2 ± 5.3 [5.6] Ma (ODP 807), and 120.1 ± 3.8 [4.1] Ma and 119.8 ± 5.2 Ma [5.5] (DSDP 317).

Summary. *Limitations*: Predominantly whole-rock or groundmass analyses, high analytical uncertainty. *Best age estimates*: Ontong Java Plateau (whole-rock): 125.3 ± 3.6 [3.9] Ma (DSDP 289) and 127.7 ± 4.5 [4.8] Ma to 122.8 ± 5.3 [5.6] Ma (ODP 807). Manihiki

Plateau (plagioclase): 119.7 ± 3.8 [4.1] Ma and 119.4 ± 5.2 [5.5] Ma (DSDP 317). All ages are from Aptian successions within the Cretaceous Normal Superchron.

4.5   High Arctic large igneous province

The High Arctic large igneous province erupted over a protracted period of time (ca. 130–80 Ma) but, importantly, the earliest eruptions overlapped with the Barremian–Aptian boundary (Buchan and Ernst, 2018; Jowitt et al., 2014). Geochronological evidence from ca. 130 to 120 Ma is available from Svalbard (Corfu et al., 2013; Midtkandal et al., 2016; Polteau et al., 2016), Franz Josef Land (Corfu et al., 2013; Shipilov and Karyakin, 2011) and northeastern Canada (Table 5, Fig. 6; Estrada and Henjes-Kunst, 2013; Evenchick et al., 2015; Villeneuve and Williamson, 2006). However, all but one of the age data are from intrusive bodies, which at best provide minimum depositional ages (Table 5). The only depositional feature is a bentonite layer from Longyearbyen (Svalbard) within a Barremian sequence, which provides the best estimate of the Barremian–Aptian boundary in the High Arctic large igneous province (Fig. 6b).

Longyearbyen in Svalbard was drilled in two proximal locations and encountered a single bentonite (clay mineral derived from the decomposition of volcanic ash) layer from the same stratigraphic interval in which zircon crystals have been dated via CA-ID-TIMS (Corfu et al., 2013; Midtkandal et al., 2016). Importantly, this bentonite layer is situated ~40 m below a major negative $\delta^{13}C$ excursion attributed to OAE1a (Midtkandal et al., 2016). Dinoflagellate biostratigraphy from a nearby well also provides important stratigraphic constraints, particularly with respect to the first occurrence of the Barremian *Simiodinium grosii* recorded ~20 m above the bentonite layer (Fig. 6b). U-Pb analyses from the two drill core samples DH3 and DH7 yielded a spread of 19 concordant dates between ca. 130 and 122 Ma (Fig. 6c) and two concordant outliers at ca. 142 and 140 Ma (not shown in Fig. 6c) that

are considered xenocrystic (Corfu et al., 2013; Midtkandal et al., 2016). Four of the older dates in the ca. 130–122 Ma age range are clearly antecrystic or xenocrystic (Fig. 6c) but the remainder of the 15 analyses form a continuum from ca. 126–122 Ma (Midtkandal et al., 2016; Siégel et al., 2018). Although the original report only utilized 9 dates to compute the age, it is possible to obtain a statistically-reliable age with the youngest 13 dates, yielding an age of 123.39 ± 0.28 [0.36] Ma (MSWD = 1.5, $p = 0.12$, Fig. 6d). As the bentonite layer was deposited during the Barremian, it is therefore only a maximum age for the Barremian–Aptian boundary and chron M0r.

Summary. *Limitations*: No magnetostratigraphy, high number of xenocrysts and antecrysts. *Best age estimates*: 123.39 ± 0.28 [0.36] Ma from uppermost Barremian.

5 BEST ESTIMATE AGE CALCULATION OF THE BARREMIAN–APTIAN BOUNDARY AND ONSET OF CHRON M0R

Of the five primary sites discussed here, two are situated in the Barremian (MIT Guyot, western Pacific and Svalbard), one within the uppermost Barremian or lowermost Aptian (Great Valley Group, California), one within chron M0r in the lowermost Aptian (Yixian Formation, China), and one region within the Cretaceous Normal Superchron (Greater Ontong Java Event). The ages from the Greater Ontong Java Event have large errors that prevent them from being useful to refine the Barremian–Aptian boundary (Fig. 7).

The two ages from the Barremian, the MIT Guyot at 123.5 ± 1.0 [1.3] Ma and Svalbard at 123.39 ± 0.28 [0.36] Ma, indicate that the Barremian–Aptian boundary must be younger than these ages. It is worth noting that the MIT Guyot ages were measured on whole-rock samples, which may notoriously hide cryptic alteration and yield younger ages (e.g., Baksi, 2007; Merle et al., 2018). Additionally, as Pringle et al. (2003) asserts, if the MIT Guyot sample is instead from the Cretaceous Normal Superchron (C34n), then it implies

that the Barremian–Aptian boundary in the MIT Guyot is at least ~0.5 Myr older (i.e., the duration of chron M0r, see section 5 and Malinverno et al., 2010). This is a distinct possibility and this may only be solved with re-dating plagioclase separates from the MIT Guyot with multi-collector $^{40}Ar/^{39}Ar$ instrumentation (e.g., ARGUS VI; Belica et al., 2017; Olierook et al., 2016; Phillips and Matchan, 2013; Ware and Jourdan, 2018), which should yield more accurate and precise ages that approach the precision of CA-ID U-Pb TIMS geochronology.

The lack of certainty in the MIT Guyot is circumvented by the high precision CA-ID-TIMS age of 123.39 ± 0.28 [0.36] Ma in Svalbard, which indicates that the Barremian–Aptian boundary can be no older than 123.8 Ma at 2σ uncertainty (including error on decay constants). The uppermost Barremian to lowermost Aptian sequence from the Great Valley Group in California provides a precise age that, on the basis of above evidence from Svalbard, implies that it is situated within the uppermost Barremian at 124.08 ± 0.15 [0.23] Ma (Shimokawa, 2010). Thus, the (probably) three Barremian sequences all suggest that the Barremian–Aptian boundary must be no older than 123.8 Ma. This indicates that the ca. 125 Ma age currently used by the International Commission on Stratigraphy for the Barremian–Aptian boundary is at least 1.2 Myr too old (Cohen et al., 2013).

The one site that is most likely within chron M0r, the Yixian Formation (China), yielded an age of 122.9 ± 0.8 [1.1] Ma (He et al., 2008). If this sample was situated in the ISEA chron, then the Barremian–Aptian boundary would have to be ~5 Myr older than 122.9 ± 0.8 [1.1] Ma (i.e. ≥ ~127.9 Ma) on the basis of cyclostratigraphy (Huang et al., 2010). Although the cyclostratigraphic estimates from Huang et al. (2010) are probably up to ~1 Myr too long (Huang, 2018), the sample dated by He et al. (2008) would still be significantly too old for the maximum age determined by the Barremian Svalbard, MIT Guyot and California sites above. Thus, we affirm that the interpretation by He et al. (2008) is probably

correct and that this sample was taken from chron M0r. This andesitic sample was measured on groundmass that, like the MIT Guyot, would benefit from re-dating using mineral separates to circumvent the possibility that the original groundmass contained cryptic alteration. On the basis of the duration of chron M0r (0.49 ± 0.10 Myr; Malinverno et al., 2010; see section 4 for duration of chron M0r), the base of M0r can be no more than 0.59 Myr (2σ) older than 122.9 ± 0.8 [1.1] Ma (Fig. 7). In lieu of mineral separate analyses (e.g. ^{40}Ar/^{39}Ar on plagioclase or U-Pb TIMS on zircon), the Barremian–Aptian can be no older than 124.3 Ma and no younger than 121.8 Ma at 2σ uncertainty as indicated by the Yixian Formation.

Using these above constraints, we conservatively infer that the Barremian–Aptian boundary is between 123.8 Ma and 121.8 Ma at 2σ confidence, including errors on decay constants (Fig. 7). Note that this age range does not imply that this is a Gaussian distribution (i.e., *not* 122.8 ± 1.0 Ma) but simply that the age of the Barremian–Aptian boundary should fall within these two ages taking into account 2σ uncertainties on the constraints. This age range should serve as the best estimate to date of the Barremian–Aptian boundary until a GSSP is formally ratified.

6 AGE AND DURATION OF THE CRETACEOUS NORMAL SUPERCHRON

The uncertainty on relative chron durations is usually significantly less than the uncertainty on the boundaries (Gradstein et al., 1994), so that the age of the onset of the Cretaceous Normal Superchron (C34n) can be readily computed using the duration of chron M0r. The duration of chron M0r was extrapolated by cyclostratigraphy at ~0.4 Myr (no statistical uncertainty) in Italy (Huang et al., 2010; Sprovieri et al., 2006). Such a duration for chron M0r was similar in the Pacific Ocean at 0.37 Myr (no statistical uncertainty; Ogg, 2012). The duration of chron M0r has been further refined using Monte Carlo simulations of

orbital tunings, which yielded a duration of 0.49 ± 0.10 Myr (2σ; Malinverno et al., 2010). Subsequent attempts to refine the duration of chron M0r by Malinverno et al. (2012) erroneously used the uncorrected dates (121.2 Ma) with an uncertainty that is too precise (± 0.5 instead of ± 0.9 Ma, 2σ) from the Liaoning Province (He et al., 2008). Therefore, the duration of chron M0r is preferentially chosen as 0.49 ± 0.10 Myr (2σ; Malinverno et al., 2010). Together with the age of the Barremian–Aptian boundary (122.8 ± 1.0 Ma), we use a Monte Carlo simulation (10,000 simulations) to calculate a conservative possible onset age of 123.4–121.2 Ma for the Cretaceous Normal Superchron

The duration of the Cretaceous Normal Superchron requires knowledge of the end of the superchron and the reappearance of magnetic reversals. Fortunately, the end of the Cretaceous Normal Superchron is far better constrained than its onset. Various studies have placed its end between ca. 84 and 83 Ma (Gradstein et al., 1994; He et al., 2012; Ogg, 2012; Sageman et al., 2014; Wang et al., 2016a). A recent study obtained a precise CA-ID-TIMS age towards the very end of the Cretaceous Normal Superchron at 83.27 ± 0.11 Ma (Wang et al., 2016a), which provides a firm maximum age. Using cyclostratigraphy and extrapolation of approximately half a ~405 Kyr eccentricity cycle, Wang et al. (2016a) assign the end of the Cretaceous Normal Superchron (chron C34y) at 83.07 ± 0.15 Ma. We suggest that, given its accuracy and precision, this age should be adopted for the end of the Cretaceous Normal Superchron.

With the onset of the Cretaceous Normal Superchron at 123.4–121.2 Ma and the cessation of the superchron at 83.07 ± 0.15 Ma, the duration of the superchron can be conservatively refined to between 38.0 and 40.5 Myr. This is equivalent to an uncertainty of ~5% on the duration of the Cretaceous Normal Superchron, which is approximately three times more precise than current estimates. Although we suspect that further geochronological evaluation of the existing sites and potential new sites will decrease this uncertainty further,

this new and more precise age range should facilitate more reliable plate velocity estimates during the Cretaceous Normal Superchron.

7   CONCLUSIONS

A re-evaluation of global geochronological data in the context of biostratigraphic and magnetostratigraphic constraints reveals that the current age of the Barremian–Aptian boundary in the Geological Time Scale and the base of chron M0r is significantly in error. Using geochronological data from the MIT Guyot, the Liaoning Province (China), California, the Ontong Java Nui large igneous province and the High Arctic large igneous province, the radioisotopic age of the Barremian–Aptian boundary and the base of chron M0r can be refined to between 123.8 and 121.8 Ma. This is a best estimate; each of the data sets used in this study have stratigraphic and/or methodological limitations.

Using the duration of chron M0r, the onset of the Cretaceous Normal Superchron can be computed to between 123.4 and 121.2 Ma. With these estimates and the end of the Superchron constrained at 83.07 ± 0.15 Ma, the duration of the Cretaceous Normal Superchron is 38.0 and 40.5 Myr, approximately three times more precise than previous estimates. Until a GSSP is formally ratified for the Barremian–Aptian boundary, we propose that these age estimates should be adopted for the Barremian–Aptian boundary (i.e., the base of chron M0r), the onset of the Cretaceous Normal Superchron and the duration of the superchron.

References

Aguirre-Urreta, B., Lescano, M., Schmitz, M.D., Tunik, M., Concheyro, A., Rawson, P.F. and Ramos, V.A., 2015. Filling the gap: new precise Early Cretaceous radioisotopic ages from the Andes. Geological Magazine, 152(3): 557-564.

Armstrong, R.L., 1978. Pre-Cenozoic Phanerozoic time scale--computer file of critical dates and consequences of new and in-progress decay-constant revisions. In: G.V. Cohee (Editor), The Geologic Time scale. AAPG Special Volumes, Tulsa, Oklahoma, pp. 73-91.

Baksi, A.K., 2006. Guidelines for assessing the reliability of ^{40}Ar/^{39}Ar plateau ages: application to ages relevant to hotspot tracks. In: G. Foulger (Editor), Mantle Plumes: discussing the origin of "hotspot" volcanism, http://www.mantleplumes.org/ArAr.html.

Baksi, A.K., 2007. A quantitative tool for detecting alteration in undisturbed rocks and minerals—I: Water, chemical weathering, and atmospheric argon. Geological Society of America Special Papers, 430: 285-303.

Baksi, A.K., Archibald, D.A. and Farrar, E., 1996. Intercalibration of 40Ar39Ar dating standards. Chemical Geology, 129(3-4): 307-324.

Bea, F., 1996. Residence of REE, Y, Th and U in Granites and Crustal Protoliths; Implications for the Chemistry of Crustal Melts. Journal of Petrology, 37(3): 521-552.

Belica, M.E., Tohver, E., Pisarevsky, S.A., Jourdan, F., Denyszyn, S. and George, A.D., 2017. Middle Permian paleomagnetism of the Sydney Basin, Eastern Gondwana: Testing Pangea models and the timing of the end of the Kiaman Reverse Superchron. Tectonophysics, 699: 178-198.

Bown, P.R., Rutledge, D.C., Crux, J.A. and Gallagher, L.T., 1998. Early Cretaceous. In: P.R. Bown (Editor), Calcareous nannofossil biostratigraphy. Chapman & Hall, British Micropalaeontological Society Publication Series, pp. 86-131.

Bralower, T.J., 1990. Lower Cretaceous calcareous nannofossil stratigraphy of the Great Valley Sequence, Sacramento Valley, California. Cretaceous research, 11(2): 101-123.

Bralower, T.J., Leckie, R.M., Sliter, W.V. and Thierstein, H.R., 1995. An integrated Cretaceous microfossil biostratigraphy. In: W.A. Berggren, D.V. Kent, M. Aubry and J. Hardenbol (Editors), Geochronology, time scales and global stratigraphic correlation. Special Publications of SEPM, Tulsa, Oklahoma, pp. 65-79.

Buchan, K.L. and Ernst, R.E., 2018. A giant circumferential dyke swarm associated with the High Arctic Large Igneous Province (HALIP). Gondwana Research, 58: 39-57.

Burke, K., Steinberger, B., Torsvik, T.H. and Smethurst, M.A., 2008. Plume Generation Zones at the margins of Large Low Shear Velocity Provinces on the core–mantle boundary. Earth and Planetary Science Letters, 265(1): 49-60.

Chambers, L.M., Pringle, M.S. and Fitton, J.G., 2004. Phreatomagmatic eruptions on the Ontong Java Plateau: an Aptian ^{40}Ar/^{39}Ar age for volcaniclastic rocks at ODP Site 1184. Geological Society, London, Special Publications, 229(1): 325-331.

Chang, S.-C., Gao, K.-Q., Zhou, C.-F. and Jourdan, F., 2017. New chronostratigraphic constraints on the Yixian Formation with implications for the Jehol Biota. Palaeogeography, Palaeoclimatology, Palaeoecology, 487: 399-406.

Chang, S.-c., Zhang, H., Renne, P.R. and Fang, Y., 2009. High-precision 40Ar/39Ar age for the Jehol Biota. Palaeogeography, Palaeoclimatology, Palaeoecology, 280(1): 94-104.

Channell, J.E.T., Erba, E., Muttoni, G. and Tremolada, F., 2000. Early Cretaceous magnetic stratigraphy in the APTICORE drill core and adjacent outcrop at Cismon (Southern Alps, Italy), and correlation to the proposed Barremian-Aptian boundary stratotype. GSA Bulletin, 112(9): 1430-1443.

Channell, J.E.T., Erba, E., Nakanishi, M. and Tamaki, K., 1995. Late Jurassic-Early Cretaceous time scales and oceanic magnetic anomaly block models, Time Scales and Global Stratigraphic Correlation. Special Publications of SEPM, pp. 51-63.

Cherniak, D.J. and Watson, E.B., 2001. Pb diffusion in zircon. Chemical Geology, 172(1): 5-24.

Cockerham, R.S. and Jarrard, R.D., 1976. 21. Paleomagnetism of some Leg 33 sediments and basalts. Deep Sea Drilling Project Reports and Publications, 33: 631-647.

Coffin, M.F., Pringle, M.S., Duncan, R.A., Gladczenko, T.P., Storey, M., Müller, R.D. and Gahagan, L.A., 2002. Kerguelen hotspot magma output since 130 Ma. Journal of Petrology, 43(7): 1121-1139.

Cohen, K.M., Finney, S.C., Gibbard, P.L. and Fan, J.X., 2013. The ICS international chronostratigraphic chart. Episodes, 36(3): 199-204.

Coleman, D.S. and Bralower, T.J., 1993. New U-Pb zircon age constraints on the Early Cretaceous time scale, Transactions, American Geophysical Union (EOS), pp. 556.

Corfu, F., Hanchar, J.M., Hoskin, P.W.O. and Kinny, P., 2003. Atlas of Zircon Textures. Reviews in Mineralogy and Geochemistry, 53(1): 469-500.

Corfu, F., Polteau, S., Planke, S., Faleide, J.I., Svensen, H., Zayoncheck, A. and Stolbov, N., 2013. U–Pb geochronology of Cretaceous magmatism on Svalbard and Franz Josef Land, Barents Sea large igneous province. Geological Magazine, 150(6): 1127-1135.

Courtillot, V. and Olson, P., 2007. Mantle plumes link magnetic superchrons to phanerozoic mass depletion events. Earth and Planetary Science Letters, 260(3-4): 495-504.

Cowie, J.W. and Bassett, M.G., 1989. International Union of Geological Sciences 1989 global stratigraphic chart with geochronometric and magnetostratigraphic calibration. Bureau of International Commission on Stratigraphy (ICS-IUGS), Ottawa, Ontario.

Davidson, J., Charlier, B., Hora, J.M. and Perlroth, R., 2005. Mineral isochrons and isotopic fingerprinting: Pitfalls and promises. Geology, 33(1): 29-32.

Dazé, A., Lee, J.K.W. and Villeneuve, M., 2003. An intercalibration study of the Fish Canyon sanidine and biotite 40Ar/39Ar standards and some comments on the age of the Fish Canyon Tuff. Chemical Geology, 199(1): 111-127.

Duncan, R.A., Hooper, P.R., Rehacek, J., Marsh, J. and Duncan, A.R., 1997. The timing and duration of the Karoo igneous event, southern Gondwana. Journal of Geophysical Research: Solid Earth, 102(B8): 18127-18138.

Erba, E., 1994. Nannofossils and superplumes: the early Aptian "nannoconid crisis". Paleoceanography, 9(3): 483-501.

Erba, E., 2004. Calcareous nannofossils and Mesozoic oceanic anoxic events. Marine Micropaleontology, 52(1): 85-106.

Erba, E., Aguado, R., Avram, E., Baraboschkin, E.J., Bergen, J.A., Bralower, T.J., Cecca, F., Channell, J.E.T., Coccioni, R. and Delanoy, G., 1996. The Aptian stage. Bulletin de l'Institut Royal des Sciences Naturelles de Belqique, Sciences de la Terre, 66(SUPPL.): 31-43.

Erba, E., Duncan, R.A., Bottini, C., Tiraboschi, D., Weissert, H., Jenkyns, H.C. and Malinverno, A., 2015. Environmental consequences of Ontong Java Plateau and Kerguelen Plateau volcanism. Geological Society of America Special Papers, 511: SPE511-15.

Erba, E., Premoli Silva, I. and Watkins, D.K., 1995. Cretaceous calcareous plankton biostratigraphy of Sites 872 through 879. In: J.A. Haggerty, I. Premoli Silva, F. Rack and M.K. McNutt (Editors), Proceedings of the Ocean Drilling Program, Scientific Results. Ocean Drilling Program, College Station, TX, pp. 157-169.

Ernst, W.G., Snow, C.A. and Scherer, H.H., 2008. Contrasting early and late Mesozoic petrotectonic evolution of northern California. GSA Bulletin, 120(1-2): 179-194.

Estrada, S. and Henjes-Kunst, F., 2013. 40Ar-39Ar and U-Pb dating of Cretaceous continental rift-related magmatism on the northeast Canadian Arctic margin [40Ar-39Ar- und U-Pb-Datierung des kretazischen kontinentalen Rift-Magmatismus am Nordostrand der kanadischen Arktis.]. Zeitschrift der Deutschen Gesellschaft für Geowissenschaften, 164(1): 107-130.

Evenchick, C.A., Davis, W.J., Bédard, J.H., Hayward, N. and Friedman, R.M., 2015. Evidence for protracted High Arctic large igneous province magmatism in the central Sverdrup Basin from stratigraphy, geochronology, and paleodepths of saucer-shaped sills. GSA Bulletin, 127(9-10): 1366-1390.

Fiet, N. and Gorin, G., 2000. Lithological expression of Milankovitch cyclicity in carbonate-dominated, pelagic, Barremian deposits in central Italy. Cretaceous Research, 21(4): 457-467.

Fiet, N., Quidelleur, X., Parize, O., Bulot, L.G. and Gillot, P.Y., 2006. Lower Cretaceous stage durations combining radiometric data and orbital chronology: Towards a more stable relative time scale? Earth and Planetary Science Letters, 246(3): 407-417.

Forster, A., Schouten, S., Baas, M. and Sinninghe Damsté, J.S., 2007. Mid-Cretaceous (Albian–Santonian) sea surface temperature record of the tropical Atlantic Ocean. Geology, 35(10): 919-922.

Frau, C., Bulot, L.G., Delanoy, G., Moreno-Bedmar, J.A., Masse, J.-P., Tendil, A.J.B. and Lanteaume, C., 2018. The Aptian GSSP candidate at Gorgo a Cerbara (Central Italy): an alternative interpretation of the bio-, litho- and chemostratigraphic markers. Newsletters on Stratigraphy, 51(3): 311-326.

Frey, F.A., Coffin, M.F., Wallace, P.J., Weis, D., Zhao, X., Wise, S.W., Wähnert, V., Teagle, D.A.H., Saccocia, P.J., Reusch, D.N., Pringle, M.S., Nicolaysen, K.E., Neal, C.R., Müller, R.D., Moore, C.L., Mahoney, J.J., Keszthelyi, L., Inokuchi, H., Duncan, R.A., Delius, H., Damuth, J.E., Damasceno, D., Coxall, H.K., Borre, M.K., Boehm, F., Barling, J., Arndt, N.T. and Antretter, M., 2000. Origin and evolution of a submarine large igneous province: the Kerguelen Plateau and Broken Ridge, southern Indian Ocean. Earth and Planetary Science Letters, 176(1): 73-89.

Gee, J. and Nakanishi, M., 1995. Magnetic petrology and magnetic properties of western Pacific guyots: implications for seamount paleopoles. In: J.A. Haggerty, I. Premoli Silva, F. Rack and M.K. McNutt (Editors), Proceeding ODP, Scientific Results. Ocean Drilling Program, College Station, Texas, pp. 615-630.

Gee, J.S. and Kent, D.V., 2007. Source of oceanic magnetic anomalies and the geomagnetic polarity time scale. Treatise on Geophysics, 5: 455-507.

Glatzmaier, G.A., Coe, R.S., Hongre, L. and Roberts, P.H., 1999. The role of the Earth's mantle in controlling the frequency of geomagnetic reversals. Nature, 401: 885.

Gradstein, F.M., Agterberg, F.P., Ogg, J.G., Hardenbol, J., Veen, P., Thierry, J. and Huang, Z., 1994. A Mesozoic time scale. Journal of Geophysical Research: Solid Earth, 99(B12): 24051-24074.

Gradstein, F.M., Ogg, J.G., Schmitz, M.D. and Ogg, G.M., (Eds.), 2012. The Geologic Time Scale 2012 2-Volume Set (Vol. 2). Elsevier, Oxford, U.K., 1176 pp.

Gradstein, F.M., Ogg, J.G., Smith, A.G., Bleeker, W. and Lourens, L.J., 2004. A new geologic time scale, with special reference to Precambrian and Neogene. Episodes, 27(2): 83-100.

Granot, R., Dyment, J. and Gallet, Y., 2012. Geomagnetic field variability during the Cretaceous Normal Superchron. Nature Geosci, 5(3): 220-223.

Hammond, S.R., Kroenke, L.W. and Theyer, F., 1975. Northward motion of the Ontong Java Plateau between 110 and 30 my: A paleomagnetic investigation of DSDP Site 289. Deep Sea Drilling Project Reports and Publications, 30: 415-418.

Haq, B.U., Hardenbol, J. and Vail, P.R., 1987. Chronology of Fluctuating Sea Levels Since the Triassic. Science, 235(4793): 1156-1167.

Harland, W.B., Armstrong, R.L., Cox, A.V., Craig, L.E., Smith, D.G. and Smith, A.G., 1990. A geologic time scale 1989. Cambridge University Press.

Harley, S.L. and Kelly, N.M., 2007. Zircon Tiny but Timely. Elements, 3(1): 13-18.

He, H., Deng, C., Wang, P., Pan, Y. and Zhu, R., 2012. Toward age determination of the termination of the Cretaceous Normal Superchron. Geochemistry, Geophysics, Geosystems, 13(2).

He, H., Pan, Y., Tauxe, L., Qin, H. and Zhu, R., 2008. Toward age determination of the M0r (Barremian–Aptian boundary) of the Early Cretaceous. Physics of the Earth and Planetary Interiors, 169(1): 41-48.

He, H.Y., Wang, X.L., Zhou, Z.H., Jin, F., Wang, F., Yang, L.K., Ding, X., Boven, A. and Zhu, R.X., 2006. 40Ar/39Ar dating of Lujiatun Bed (Jehol Group) in Liaoning, northeastern China. Geophysical Research Letters, 33(4).

He, H.Y., Wang, X.L., Zhou, Z.H., Wang, F., Boven, A., Shi, G.H. and Zhu, R.X., 2004. Timing of the Jiufotang Formation (Jehol Group) in Liaoning, northeastern China, and its implications. Geophysical Research Letters, 31(12).

Helsley, C.E. and Steiner, M.B., 1968. Evidence for long intervals of normal polarity during the cretaceous period. Earth and Planetary Science Letters, 5: 325-332.

Hide, R., 2000. Generic nonlinear processes in self–exciting dynamos and the long–term behaviour of the main geomagnetic field, including polarity superchrons.

Philosophical Transactions of the Royal Society of London A: Mathematical, Physical and Engineering Sciences, 358(1768): 943-955.

Hiess, J., Condon, D.J., McLean, N. and Noble, S.R., 2012. 238U/235U systematics in terrestrial uranium-bearing minerals. Science, 335(6076): 1610-1614.

Hoedemaker, P.J., Reboulet, S., Aguirre-Urreta, M.B., Alsen, P., Autem, M., Atrops, F., Barragan, R., Arreola, C.G., Klein, J., Lukeneder, A., Ploch, I., Raisossadat, N., Rawson, P.F., Ropolo, P., Vasicek, Z., Vermeulen, J. and Wippich, M.G.E., 2003. Report of the 1st International Workshop of the IUGS Lower Cretaceous Ammonite Working Group. Cretaceous Research, 24: 89-94.

Hoernle, K., Hauff, F., van den Bogaard, P., Werner, R., Mortimer, N., Geldmacher, J., Garbe-Schönberg, D. and Davy, B., 2010. Age and geochemistry of volcanic rocks from the Hikurangi and Manihiki oceanic Plateaus. Geochimica et Cosmochimica Acta, 74(24): 7196-7219.

Hofmann, C., Féraud, G. and Courtillot, V., 2000. 40Ar/39Ar dating of mineral separates and whole rocks from the Western Ghats lava pile: further constraints on duration and age of the Deccan traps. Earth and Planetary Science Letters, 180(1): 13-27.

Huang, C., 2018. Chapter Two - Astronomical Time Scale for the Mesozoic. In: M. Montenari (Editor), Stratigraphy & Timescales. Academic Press, pp. 81-150.

Huang, C., Hinnov, L., Fischer, A.G., Grippo, A. and Herbert, T., 2010. Astronomical tuning of the Aptian Stage from Italian reference sections. Geology, 38(10): 899-902.

Ingle, S., Mahoney, J.J., Sato, H., Coffin, M.F., Kimura, J.-I., Hirano, N. and Nakanishi, M., 2007. Depleted mantle wedge and sediment fingerprint in unusual basalts from the Manihiki Plateau, central Pacific Ocean. Geology, 35(7): 595-598.

Jacobs, J.A., 2001. The cause of superchrons. Astronomy & Geophysics, 42(6): 6-30.

Jenkyns, H.C., 2010. Geochemistry of oceanic anoxic events. Geochemistry, Geophysics, Geosystems, 11(3).

Jenkyns, H.C., Jones, C.E., Grocke, D.R., Hesselbo, S.P. and Parkinson, D.N., 2002. Chemostratigraphy of the Jurassic System: applications, limitations and implications for palaeoceanography. Journal of the Geological Society, 159: 351-378.

Jourdan, F., Féraud, G., Bertrand, H., Watkeys, M. and Renne, P., 2007. Distinct brief major events in the Karoo large igneous province clarified by new 40Ar/39Ar ages on the Lesotho basalts. Lithos, 98: 195-209.

Jourdan, F. and Renne, P.R., 2007. Age calibration of the Fish Canyon sanidine 40Ar/39Ar dating standard using primary K-Ar standards. Geochimica et Cosmochimica Acta, 71(2): 387-402.

Jowitt, S.M., Williamson, M.-C. and Ernst, R.E., 2014. Geochemistry of the 130 to 80 Ma Canadian High Arctic large igneous province (HALIP) event and implications for Ni-Cu-PGE prospectivity. Economic Geology, 109(2): 281-307.

Karpuk, M.S., Shcherbinina, E.A., A., B.E., Aleksandrova, G.N., Guzhikov, A.Y., Shchepetova, E.V. and Tesakova, E.M., 2018. Integrated stratigraphy of the Upper Barremian–Aptian sediments from the south-eastern Crimea. Geologica Carpathica, 69(5): 498-511.

Kelley, S., 2002. Excess argon in K–Ar and Ar–Ar geochronology. Chemical Geology, 188(1): 1-22.

Kendall, J.M. and Silver, P.G., 1996. Constraints from seismic anisotropy on the nature of the lowermost mantle. Nature, 381(6581): 409.

Kent, D.V., Olsen, P.E., Rasmussen, C., Lepre, C., Mundil, R., Irmis, R.B., Gehrels, G.E., Giesler, D., Geissman, J.W. and Parker, W.G., 2018. Empirical evidence for stability of the 405-kiloyear Jupiter–Venus eccentricity cycle over hundreds of millions of years. Proceedings of the National Academy of Sciences, 115(24): 6153-6158.

Kirkland, C.L., Hollis, J., Danišík, M., Petersen, J., Evans, N.J. and McDonald, B.J., 2017. Apatite and titanite from the Karrat Group, Greenland; implications for charting the thermal evolution of crust from the U-Pb geochronology of common Pb bearing phases. Precambrian Research, 300(Supplement C): 107-120.

Koppers, A.A.P., Staudigel, H., Christie, D.M., Dieu, J.J. and Pringle, M.S., 1995. Sr-Nd-Pb isotope geochemistry of Leg 144 west Pacific guyots: implications for the geochemical evolution of the" SOPITA" mantle anomaly. In: J.A. Haggerty, I. Premoli Silva, F. Rack and M.K. McNutt (Editors), Proceeding ODP, Scientific Results. Ocean Drilling Program, College Station, Texas, pp. 535-545.

Koppers, A.A.P., Staudigel, H., Wijbrans, J.R. and Pringle, M.S., 1998. The Magellan seamount trail: implications for Cretaceous hotspot volcanism and absolute Pacific plate motion. Earth and Planetary Science Letters, 163(1): 53-68.

Kuiper, K.F., Deino, A., Hilgen, F.J., Krijgsman, W., Renne, P.R., Wijbrans and Jr, 2008. Synchronizing rock clocks of Earth history. science, 320(5875): 500-504.

Larson, R.L. and Erba, E., 1999. Onset of the Mid-Cretaceous greenhouse in the Barremian-Aptian: Igneous events and the biological, sedimentary, and geochemical responses. Paleoceanography, 14(6): 663-678.

Larson, R.L. and Olson, P., 1991. Mantle plumes control magnetic reversal frequency. Earth and Planetary Science Letters, 107(3-4): 437-447.

Leckie, R.M., Bralower, T.J. and Cashman, R., 2002. Oceanic anoxic events and plankton evolution: Biotic response to tectonic forcing during the mid-Cretaceous. Paleoceanography, 17(3): 13-1-13-29.

Lee, J.-Y., Marti, K., Severinghaus, J.P., Kawamura, K., Yoo, H.-S., Lee, J.B. and Kim, J.S., 2006. A redetermination of the isotopic abundances of atmospheric Ar. Geochimica et Cosmochimica Acta, 70(17): 4507-4512.

Lee, J.K.W., Williams, I.S. and Ellis, D.J., 1997. Pb, U and Th diffusion in natural zircon. Nature, 390: 159-162.

Mahoney, J.J., Storey, M., Duncan, R.A., Spencer, K.J. and Pringle, M., 1993. Geochemistry and age of the Ontong Java Plateau. The Mesozoic Pacific: Geology, Tectonics, and Volcanism, Geophys. Monogr. Ser, 77: 233-261.

Malinverno, A., Erba, E. and Herbert, T.D., 2010. Orbital tuning as an inverse problem: Chronology of the early Aptian oceanic anoxic event 1a (Selli Level) in the Cismon APTICORE. Paleoceanography, 25(2).

Malinverno, A., Hildebrandt, J., Tominaga, M. and Channell, J.E.T., 2012. M-sequence geomagnetic polarity time scale (MHTC12) that steadies global spreading rates and incorporates astrochronology constraints. Journal of Geophysical Research: Solid Earth, 117(B6).

Mao, S. and Wise, S.W.J., 1993. Mesozoic calcareous nannofossils from Leg 130. Proceedings of the Ocean Drilling Program, Scientific Results, 130: 85-92.

Matthews, K.J., Seton, M. and Müller, R.D., 2012. A global-scale plate reorganization event at 105−100 Ma. Earth and Planetary Science Letters, 355–356(0): 283-298.

Mattinson, J.M., 2005. Zircon U–Pb chemical abrasion ("CA-TIMS") method: Combined annealing and multi-step partial dissolution analysis for improved precision and accuracy of zircon ages. Chemical Geology, 220(1): 47-66.

McDougall, I., Mac Dougall, I. and Harrison, T.M., 1999. Geochronology and Thermochronology by the 40Ar/39Ar Method. Oxford University Press.

McNulty, C.L., 1976. Cretaceous foraminiferal stratigraphy, DSDP Leg 33, Holes 315A, 317a. Deep Sea Drilling Project Reports and Publications, 33: 369-381.

Merle, R., Jourdan, F. and Girardeau, J., 2018. Geochronology of the Tore-Madeira Rise seamounts and surrounding areas: a review. Australian Journal of Earth Sciences, 65(5): 591-605.

Merle, R., Jourdan, F., Marzoli, A., Renne, P.R., Grange, M. and Girardeau, J., 2009. Evidence of multi-phase Cretaceous to Quaternary alkaline magmatism on Tore–Madeira Rise and neighbouring seamounts from ^{40}Ar/^{39}Ar ages. Journal of the Geological Society, 166(5): 879-894.

Merle, R.E., Jourdan, F., Chiaradia, M., Olierook, H.K.H. and Manatschal, G., 2019. Origin of widespread Cretaceous alkaline magmatism in the Central Atlantic: A single melting anomaly? Lithos, 342-343: 480-498.

Michael, F.Y., 1975. Mesozoic foraminifera, Leg 30, Hole 288A And Site 289. Deep Sea Drilling Project Reports and Publications, 30: 599-601.

Midtkandal, I., Svensen, H.H., Planke, S., Corfu, F., Polteau, S., Torsvik, T.H., Faleide, J.I., Grundvåg, S.-A., Selnes, H., Kürschner, W. and Olaussen, S., 2016. The Aptian (Early Cretaceous) oceanic anoxic event (OAE1a) in Svalbard, Barents Sea, and the absolute age of the Barremian-Aptian boundary. Palaeogeography, Palaeoclimatology, Palaeoecology, 463: 126-135.

Min, K., Mundil, R., Renne, P.R. and Ludwig, K.R., 2000. A test for systematic errors in ^{40}Ar/^{39}Ar geochronology through comparison with U–Pb analysis of a 1.1 Ga rhyolite. Geochimica et Cosmochimica Acta, 64: 73-98.

Mortimer, N. and Parkinson, D., 1996. Hikurangi Plateau: A Cretaceous large igneous province in the southwest Pacific Ocean. Journal of Geophysical Research: Solid Earth, 101(B1): 687-696.

Moullade, M., Granier, B. and Tronchetti, G., 2011. The Aptian stage: Back to fundamentals. Episodes, 34(3): 148-156.

Moullade, M., Masse, J.-P., Tronchetti, G., Kuhnt, W., Ropolo, P., Bergen, J.A., Masure, E. and Renard, M., 1998a. Le stratotype historique de l'Aptien inférieur (région de Cassis-La Bédoule): synthèse stratigraphique. Géologie méditerranéenne, 25(3): 289-298.

Moullade, M., Tronchetti, G. and Masse, J.P., 1998b. Le stratotype historique de l'Aptien inférieur (Bédoulien) dans la région de Cassis-La Bédoule (SE France). Géologie Méditerranéenne. Marseille.

Müller, R.D., Seton, M., Zahirovic, S., Williams, S.E., Matthews, K.J., Wright, N.M., Shephard, G.E., Maloney, K.T., Barnett-Moore, N., Hosseinpour, M., Bower, D.J. and Cannon, J., 2016. Ocean Basin Evolution and Global-Scale Plate Reorganization Events Since Pangea Breakup. Annual Review of Earth and Planetary Sciences, 44(1): 107-138.

Musgrave, R.J., Delaney, M.L., Stax, R. and Tarduno, J.A., 1993. Magnetic diagenesis, organic input, interstitial water chemistry, and paleomagnetic record in the carbonate sequence on the Ontong-Java-Plateau. Proceedings of the Ocean Drilling Program, Scientific Results, 130: 527-546.

Neal, C.R., Coffin, M.F., Arndt, N.T., Duncan, R.A., Eldholm, O., Erba, E., Farnetani, C., Fitton, J.F., Ingle, S.P. and Ohkouchi, N., 2008. Investigating large igneous province formation and associated paleoenvironmental events: a white paper for scientific drilling. Scientific Drilling, 6: 4-18.

Odin, G.S., 1990. Echelle numérique des temps géologiques. Geochronologie, 35: 12-20.

Ogg, J.G., 2012. Chapter 5 - Geomagnetic Polarity Time Scale, The Geologic Time Scale. Elsevier, Boston, pp. 85-113.

Ogg, J.G., Hinnov, L.A. and Huang, C., 2012. Chapter 27 - Cretaceous. In: F.M. Gradstein, J.G. Ogg, M.D. Schmitz and G.M. Ogg (Editors), The Geologic Time Scale. Elsevier, Boston, pp. 793-853.

Ogg, J.G., Ogg, G. and Gradstein, F.M., 2016a. A concise geologic time scale: 2016. Elsevier.

Ogg, J.G., Ogg, G.M. and Gradstein, F.M., 2016b. 13 - Cretaceous. In: J.G. Ogg, G.M. Ogg and F.M. Gradstein (Editors), A Concise Geologic Time Scale. Elsevier, pp. 167-186.

Ogg, J.G. and Smith, A., 2004. The geomagnetic polarity timescale. In: F.M. Gradstein, J.G. Ogg and A. Smith (Editors), A Geologic Time Scale. Cambridge University Press, pp. 589.

Olierook, H.K.H., Agangi, A., Plavsa, D., Reddy, S.M., Clark, C., Yao, W.-H., Occhipinti, S.A. and Kylander-Clark, A.R.C., 2019a. Neoproterozoic hydrothermal activity in the West Australian Craton related to Rodinia assembly or breakup? Gondwana Research, 68: 1-12.

Olierook, H.K.H., Clark, C., Reddy, S.M., Mazumder, R., Jourdan, F. and Evans, N.J., 2019b. Evolution of the Singhbhum Craton and supracrustal province from age, isotopic and chemical constraints. Earth-Science Reviews, 193: 237-259.

Olierook, H.K.H., Jiang, Q., Jourdan, F. and Chiaradia, M., 2019c. Greater Kerguelen large igneous province reveals no role for Kerguelen mantle plume in the continental breakup of eastern Gondwana. Earth and Planetary Science Letters, 511: 244-255.

Olierook, H.K.H., Jourdan, F., Merle, R.E., Timms, N.E., Kusznir, N.J. and Muhling, J., 2016. Bunbury Basalt: Gondwana breakup products or earliest vestiges of the Kerguelen mantle plume? Earth and Planetary Science Letters, 440: 20-32.

Olierook, H.K.H., Merle, R.E. and Jourdan, F., 2017. Toward a Greater Kerguelen large igneous province: Evolving mantle source contributions in and around the Indian Ocean. Lithos, 282–283: 163-172.

Olierook, H.K.H., Merle, R.E., Jourdan, F., Sircombe, K., Fraser, G., Timms, N.E., Nelson, G., Dadd, K.A., Kellerson, L. and Borissova, I., 2015. Age and geochemistry of

magmatism on the oceanic Wallaby Plateau and implications for the opening of the Indian Ocean. Geology, 43: 971-974.

Olierook, H.K.H., Sheppard, S., Johnson, S.P., Occhipinti, S.A., Reddy, S.M., Clark, C., Fletcher, I.R., Rasmussen, B., Zi, J.-W., Pirajno, F., LaFlamme, C., Do, T., Ware, B., Blandthorn, E., Lindsay, M., Lu, Y.-J., Crossley, R.J. and Erickson, T.M., 2018. Extensional episodes in the Paleoproterozoic Capricorn Orogen, Western Australia, revealed by petrogenesis and geochronology of mafic–ultramafic rocks. Precambrian Research, 306: 22-40.

Olierook, H.K.H., Taylor, R.J.M., Erickson, T.M., Clark, C., Reddy, S.M., Kirkland, C.L., Jahn, I. and Barham, M., 2019d. Unravelling complex geologic histories using U–Pb and trace element systematics of titanite. Chemical Geology, 504: 105-122.

Olson, P.L., Christensen, U.R. and Driscoll, P.E., 2012. From superchrons to secular variation: A broadband dynamo frequency spectrum for the geomagnetic dipole. Earth and Planetary Science Letters, 319: 75-82.

Opdyke, M.D. and Channell, J.E.T., 1996. Magnetic stratigraphy, 64. Academic press.

Orbigny, A.d., 1840. Paléontologie Française. Tome I, Terrains crétacés, Céphalopodes. Publ. Arthus Bertrand, Paris.

Palmer, A.R., 1983. The decade of North American geology 1983 geologic time scale. Geology, 11(9): 503-504.

Phillips, D. and Matchan, E., 2013. Ultra-high precision 40 Ar/39 Ar ages for Fish Canyon Tuff and Alder Creek Rhyolite sanidine: New dating standards required? Geochimica et Cosmochimica Acta, 121: 229-239.

Piechocka, A.M., Gregory, C.J., Zi, J.-W., Sheppard, S., Wingate, M.T.D. and Rasmussen, B., 2017. Monazite trumps zircon: applying SHRIMP U–Pb geochronology to systematically evaluate emplacement ages of leucocratic, low-temperature granites in a complex Precambrian orogen. Contributions to Mineralogy and Petrology, 172(8): 63.

Polteau, S., Hendriks, B.W.H., Planke, S., Ganerød, M., Corfu, F., Faleide, J.I., Midtkandal, I., Svensen, H.S. and Myklebust, R., 2016. The Early Cretaceous Barents Sea Sill Complex: Distribution, 40Ar/39Ar geochronology, and implications for carbon gas formation. Palaeogeography, Palaeoclimatology, Palaeoecology, 441: 83-95.

Premoli Silva, I., Nicora, A., Arnaud Vanneau, A., Budd, A.F., Camoin, G.F. and Masse, J.-P., 1995. Paleobiogeographic evolution of shallow-water organisms from the Aptian to the Eocene in the western Pacific. In: J.A. Haggerty, I. Premoli Silva, F. Rack and M.K. McNutt (Editors), Proceedings of the Ocean Drilling Program, Scientific Results. Ocean Drilling Program, College Station, TX, pp. 887-893.

Pringle, M., Chambers, L. and Ogg, J., 2003. Synchronicity of volcanism on Ontong Java and Manihiki Plateaux with global oceanographic events?, EGS-AGU-EUG Joint Assembly, Nice, France.

Pringle, M.S. and Duncan, R.A., 1995. Radiometric ages of basement lavas recovered at Loen, Wodejebato, MIT, and Takuyo-Daisan Guyots, northwestern Pacific Ocean. Proceedings of the Ocean Drilling Program, Scientific Results, 144: 547-557.

Pringle, M.S., Storey, M. and Wijbrans, J., 1994. $^{40}Ar/^{39}Ar$ geochronology of mid-Cretaceous Indian Ocean basalts: Constraints on the origin of large flood basalt provinces. EOS, Transactions of the American Geophysical Union, 75: 728.

Rawson, P.F., 1983. The Valanginian to Aptian stages—current definitions and outstanding problems. Zitteliana, 10: 493-500.

Reboulet, S., Rawson, P.F., Moreno-Bedmar, J.A., Aguirre-Urreta, M.B., Barragán, R., Bogomolov, Y., Company, M., González-Arreola, C., Stoyanova, V.I. and Lukeneder, A., 2011. Report on the 4th international meeting of the IUGS Lower Cretaceous ammonite working group, the "Kilian Group"(Dijon, France, 30th August 2010). Cretaceous Research, 32(6): 786-793.

Renne, P.R., Balco, G., Ludwig, K.R., Mundil, R. and Min, K., 2011. Response to the comment by W.H. Schwarz et al. on "Joint determination of ^{40}K decay constants and $^{40}Ar*/^{40}K$ for the Fish Canyon sanidine standard, and improved accuracy for $^{40}Ar/^{39}Ar$ geochronology" by PR Renne et al. (2010). Geochimica et Cosmochimica Acta, 75: 5097-5100.

Renne, P.R., Mundil, R., Balco, G., Min, K. and Ludwig, K.R., 2010. Joint determination of ^{40}K decay constants and $^{40}Ar*/^{40}K$ for the Fish Canyon sanidine standard, and improved accuracy for $^{40}Ar/^{39}Ar$ geochronology. Geochimica et Cosmochimica Acta, 74(18): 5349-5367.

Renne, P.R., Swisher, C.C., Deino, A.L., Karner, D.B., Owens, T.L. and DePaolo, D.J., 1998. Intercalibration of standards, absolute ages and uncertainties in $^{40}Ar/^{39}Ar$ dating. Chemical Geology, 145(1–2): 117-152.

Sageman, B.B., Singer, B.S., Meyers, S.R., Siewert, S.E., Walaszczyk, I., Condon, D.J., Jicha, B.R., Obradovich, J.D. and Sawyer, D.A., 2014. Integrating 40Ar/39Ar, U-Pb, and astronomical clocks in the Cretaceous Niobrara Formation, Western Interior Basin, USA. GSA Bulletin, 126(7-8): 956-973.

Santosh, M., 2010. Supercontinent tectonics and biogeochemical cycle: A matter of 'life and death'. Geoscience Frontiers, 1(1): 21-30.

Seton, M., Gaina, C., Müller, R.D. and Heine, C., 2009. Mid-Cretaceous seafloor spreading pulse: Fact or fiction? Geology, 37(8): 687-690.

Seton, M., Müller, R.D., Zahirovic, S., Gaina, C., Torsvik, T., Shephard, G., Talsma, A., Gurnis, M., Turner, M., Maus, S. and Chandler, M., 2012. Global continental and ocean basin reconstructions since 200 Ma. Earth-Science Reviews, 113(3–4): 212-270.

Shimokawa, A., 2010. Zircon U-Pb Geochronology of the Great Valley Group: Recalibrating the Lower Cretaceous Time Scale, University of North Carolina, Chapel Hill, 46 pp.

Shipilov, E.V. and Karyakin, Y.V., 2011. The barents sea magmatic province: Geological-geophysical evidence and new 40Ar/39Ar dates. Doklady Earth Sciences, 439(1): 955.

Siégel, C., Bryan, S.E., Allen, C.M. and Gust, D.A., 2018. Use and abuse of zircon-based thermometers: A critical review and a recommended approach to identify antecrystic zircons. Earth-Science Reviews, 176: 87-116.

Sikora, P.J. and Bergen, J.A., 2004. Lower Cretaceous planktonic foraminiferal and nannofossil biostratigraphy of Ontong Java Plateau sites from DSDP Leg 30 and ODP Leg 192. Geological Society, London, Special Publications, 229(1): 83-111.

Sliter, W.V. and Leckie, R.M., 1993. Cretaceous planktonic foraminifers and depositional environments from the Ontong Java Plateau with emphasis on Sites 803 and 807. Proceedings of the Ocean Drilling Program, Scientific Results, 130: 63-84.

Smith, P.E., Evensen, N.M., York, D., Chang, M.-M., Jin, F., Li, J.-L., Cumbaa, S. and Russell, D., 1995. Dates and rates in ancient lakes: 40Ar–39Ar evidence for an Early Cretaceous age for the Jehol Group, northeast China. Canadian Journal of Earth Sciences, 32(9): 1426-1431.

Speer, J.A., 1980. Zircon. In: P.H. Ribbe (Editor), Orthosilicates, Reviews in Mineralogy. Mineralogical Society of America, Washington, DC, pp. 67-112.

Spencer, C.J., Kirkland, C.L. and Taylor, R.J.M., 2016. Strategies towards statistically robust interpretations of in situ U–Pb zircon geochronology. Geoscience Frontiers, 7(4): 581-589.

Sprovieri, M., Coccioni, R., Lirer, F., Pelosi, N. and Lozar, F., 2006. Orbital tuning of a lower Cretaceous composite record (Maiolica Formation, central Italy). Paleoceanography and Paleoclimatology, 21(4).

Steiger, R.H. and Jäger, E., 1977. Subcommission on geochronology: convention on the use of decay constants in geo- and cosmochronology. Earth and Planetary Science Letters, 36: 359-362.

Steinberger, B., 2000. Plumes in a convecting mantle- Models and observations for individual hotspots. Journal of Geophysical Research, 105(B5): 11,127-11,152.

Swisher, C.C., Wang, Y.-q., Wang, X.-l., Xu, X. and Wang, Y., 1999. Cretaceous age for the feathered dinosaurs of Liaoning, China. Nature, 400: 58.

Takahashi, K. and Ling, H.Y., 1993. Cretaceous radiolarians from the Ontong Java Plateau, western Pacific, holes 803D and 807C. Proceedings of the Ocean Drilling Program, Scientific Results, 130: 93-102.

Tarduno, J.A., 1990. Brief reversed polarity interval during the Cretaceous normal polarity superchron. Geology, 18(8): 683-686.

Tarduno, J.A., Sliter, W.V., Kroenke, L., Leckie, M., Mayer, H., Mahoney, J.J., Musgrave, R., Storey, M. and Winterer, E.L., 1991. Rapid formation of Ontong Java Plateau by Aptian mantle plume volcanism. Science, 254(5030): 399-403.

Taylor, B., 2006. The single largest oceanic plateau: Ontong Java–Manihiki–Hikurangi. Earth and Planetary Science Letters, 241(3–4): 372-380.

Tejada, M.L.G., Mahoney, J.J., Duncan, R.A. and Hawkins, M.P., 1996. Age and geochemistry of basement and alkalic rocks of Malaita and Santa Isabel, Solomon Islands, southern margin of Ontong Java Plateau. Journal of Petrology, 37(2): 361-394.

Tejada, M.L.G., Mahoney, J.J., Neal, C.R., Duncan, R.A. and Petterson, M.G., 2002. Basement geochemistry and geochronology of Central Malaita, Solomon Islands, with implications for the origin and evolution of the Ontong Java Plateau. Journal of Petrology, 43(3): 449-484.

Timm, C., Hoernle, K., Werner, R., Hauff, F., den Bogaard, P.v., Michael, P., Coffin, M.F. and Koppers, A., 2011. Age and geochemistry of the oceanic Manihiki Plateau, SW Pacific: New evidence for a plume origin. Earth and Planetary Science Letters, 304(1): 135-146.

Vennari, V.V., Lescano, M., Naipauer, M., Aguirre-Urreta, B., Concheyro, A., Schaltegger, U., Armstrong, R., Pimentel, M. and Ramos, V.A., 2014. New constraints on the Jurassic–Cretaceous boundary in the High Andes using high-precision U–Pb data. Gondwana Research, 26(1): 374-385.

Verati, C. and Jourdan, F., 2014. Modelling effect of sericitization of plagioclase on the $^{40}K/^{40}Ar$ and $^{40}K/^{39}Ar$ chronometers: Implication for dating basaltic rocks and mineral deposits. Geological Society Special Publication, 378(1): 155-174.

Villeneuve, M. and Williamson, M.C., 2006. 40Ar-39Ar dating of mafic magmatism from the Sverdrup Basin magmatic province. Proceedings of the Fourth International Conference on Arctic Margins: 206-215.

Wang, S., Wang, Y., Hu, H. and Li, H., 2001a. The existing time of Sihetun vertebrate in western Liaoning, China. Chinese Science Bulletin, 46(9): 779-782.

Wang, S.S., Hu, H.G., Li, P.X. and Wang, Y.Q., 2001b. Further discussion on the geologic age of Sihetun vertebrate assemblage in western Liaoning, China: evidence from Ar-Ar dating. Acta Petrologica Sinica, 4: 663-668.

Wang, T., Ramezani, J., Wang, C., Wu, H., He, H. and Bowring, S.A., 2016a. High-precision U–Pb geochronologic constraints on the Late Cretaceous terrestrial cyclostratigraphy and geomagnetic polarity from the Songliao Basin, Northeast China. Earth and Planetary Science Letters, 446: 37-44.

Wang, X.L., Wang, Y.Q., Wang, Y., Wang, Y., Xu, X., Tang, Z., Zhang, F., Hu, Y., Gu, G. and Hao, Z., 1989. Stratigraphic sequence Jianshangou Bed of the Yixian Formation in West Liaoning, China and vertebrate-bearing beds of the lower part of the Yixian Formation in Sihetun and neighboring area, western Liaoning, China. Vertebrata PalAsiatica, 36(2): 81-101 (in Chinese).

Wang, Y., Olsen, P.E., Sha, J., Yao, X., Liao, H., Pan, Y., Kinney, S., Zhang, X. and Rao, X., 2016b. Stratigraphy, correlation, depositional environments, and cyclicity of the Early Cretaceous Yixian and ?Jurassic-Cretaceous Tuchengzi formations in the Sihetun area (NE China) based on three continuous cores. Palaeogeography, Palaeoclimatology, Palaeoecology, 464: 110-133.

Ware, B. and Jourdan, F., 2018. 40Ar/39Ar geochronology of terrestrial pyroxene. Geochimica et Cosmochimica Acta, 230: 112-136.

Watson, E.B., Chemiak, D.J., Hanchar, J.M., Harrison, T.M. and Wark, D.A., 1997. The incorporation of Pb into zircon. Chemical Geology, 141(1): 19-31.

Wingate, M.T.D. and Giddings, J.W., 2000. Age and palaeomagnetism of the Mundine Well dyke swarm, Western Australia: implications for an Australia–Laurentia connection at 755 Ma. Precambrian Research, 100(1–3): 335-357.

Wissler, L., Weissert, H., Masse, J.-P. and Bulot, L., 2002. Chemostratigraphic correlation of Barremian and lower Aptian ammonite zones and magnetic reversals. International Journal of Earth Sciences, 91(2): 272-279.

Yang, W., Li, S. and Jiang, B., 2007. New evidence for Cretaceous age of the feathered dinosaurs of Liaoning: zircon U-Pb SHRIMP dating of the Yixian Formation in Sihetun, northeast China. Cretaceous Research, 28(2): 177-182.

York, D., 1966. Least-squares fitting of a straight line. Canadian Journal of Physics, 44(5): 1079-1086.

York, D., 1969. Least squares fitting of a straight line with correlated errors. Earth and planetary science letters, 5: 320-324.

Young, A., Flament, N., Maloney, K., Williams, S., Matthews, K., Zahirovic, S. and Müller, R.D., 2018. Global kinematics of tectonic plates and subduction zones since the late Paleozoic Era. Geoscience Frontiers.

Zhu, R., Hoffman, K.A., Nomade, S., Renne, P.R., Shi, R., Pan, Y. and Shi, G., 2004. Geomagnetic paleointensity and direct age determination of the ISEA (M0r?) chron. Earth and Planetary Science Letters, 217(3): 285-295.

Table 1: Summary of $^{40}Ar/^{39}Ar$ results for normally- and reversely-polarized lava flows (M1n–M1r?) in the MIT Guyot (Pringle and Duncan, 1995). Bold ages indicate reliable age constraints. Ages recalculated using decay constants and intercalibration ratios of Renne et al. (2011).

Stratigraphic Position	Sample Name	Lithology	Method	Mineral	Original Age (Ma ± 2σ)	^{39}Ar in plateau	MSWD	p	n	Standard	Original standard age (Ma ± 1σ)	Original Decay Constant (λ$_ε$+λ$_β$)	New standard age (Ma ± 2σ)	Recalculated age (Ma ± 2σ [inc. decay constants])	Source
ODP Site 878, MIT Guyot, western Pacific Ocean															
Upper lava flow, near top M1n	46M-1, 115-119	Hawaiite	$^{40}Ar/^{39}Ar$ plateau	Whole-rock	121.4 ± 1.4	91	?	>0.05	5 of 7	85G003 TCR sanidine	27.92 ± 0.04	5.543 E-10	28.608 ± 0.033	124.3 ± 1.4 [1.7]	Pringle and Duncan (1995)
Upper lava flow, near top M1n	46M-2, 51-55	Hawaiite	$^{40}Ar/^{39}Ar$ plateau	Whole-rock	119.9 ± 2.6	71	?	>0.05	5 of 7	85G003 TCR sanidine	27.92 ± 0.04	5.543 E-10	28.608 ± 0.033	122.8 ± 2.6 [2.9]	Pringle and Duncan (1995)
Upper lava flow, near top M1n	79R-3, 103-109	Hawaiite	$^{40}Ar/^{39}Ar$ plateau	Whole-rock	119.9 ± 1.6	59	?	>0.05	5 of 7	85G003 TCR sanidine	27.92 ± 0.04	5.543 E-10	28.608 ± 0.033	122.8 ± 1.6 [1.9]	Pringle and Duncan (1995)
							1.18	0.31	3 of 3 samples				**Weighted mean**	**123.5 ± 1.0 [1.3]**	
Middle lava flow, middle of M1n	80R-6, 94-98	Basanite	$^{40}Ar/^{39}Ar$ plateau	Whole-rock	118.5 ± 2.0	86	?	>0.05	3 of 6	85G003 TCR sanidine	27.92 ± 0.04	5.543 E-10	28.608 ± 0.033	**121.4 ± 2.0 [2.3]**	Pringle and Duncan (1995)
Lower lava flow, M1n-M1r transition	89R-4, 33-37	Alkali Basalt	$^{40}Ar/^{39}Ar$ plateau	Whole-rock	124.4 ± 1.4	66	?	>0.05	5 of 8	85G003 TCR sanidine	27.92 ± 0.04	5.543 E-10	28.608 ± 0.033	127.4 ± 1.4 [1.7]	Pringle and Duncan (1995)
Lower lava flow, M1n-M1r transition	91R-3, 100-106	Alkali Basalt	$^{40}Ar/^{39}Ar$ plateau	Whole-rock	123.9 ± 1.4	70	?	>0.05	3 of 6	85G003 TCR sanidine	27.92 ± 0.04	5.543 E-10	28.608 ± 0.033	126.9 ± 1.4 [1.7]	Pringle and Duncan (1995)
Lower lava flow, M1n-M1r transition	98R-3, 48-53	Alkali Basalt	$^{40}Ar/^{39}Ar$ plateau	Whole-rock	123.6 ± 1.4	73	?	>0.05	5 of 8	85G003 TCR sanidine	27.92 ± 0.04	5.543 E-10	28.608 ± 0.033	126.6 ± 1.4 [1.7]	Pringle and Duncan (1995)
							0.35	0.71	3 of 3 samples				**Weighted mean**	**127.0 ± 0.8 [1.1]**	

Table 2: Summary of geochronological data from the Yixian Formation and overlying lowermost Jiufotang Formation in the Liaoning Province, China. Bold ages indicate reliable age constraints. U-Pb data recalculated using decay constants of Steiger and Jäger (1977) and $^{238}U/^{235}U$ ratio of 137.82 (Hiess et al., 2012). $^{40}Ar/^{39}Ar$ data recalculated using decay constants and intercalibration ratios of Renne et al. (2011).

Stratigraphic Position	Sample Name	Lithology	Method	Mineral	Original Age (Ma ± 2σ)	^{39}Ar in plateau	MSWD	p	n	Standard	Original standard age (Ma ± 1σ)	Original Decay Constant ($\lambda_\varepsilon + \lambda_\delta$)	New standard age (Ma ± 2σ)	Recalculated age (Ma ± 2σ [inc. decay constants])	Source
Jiufotang Formation															
Jianguo section, ISEA?	JG13	Andesite	$^{40}Ar/^{39}Ar$ plateau	Groundmass	118.9 ± 1.1	75	1	0.46	19	FC sanidine	28.02 ± 0.28	5.543E-10	28.294 ± 0.036	**120.0 ± 1.1 [1.4]**	Zhu et al. (2004)
Lower part of formation	LX9	Tuff	$^{40}Ar/^{39}Ar$ plateau	Sanidine & orthoclase	120.1 ± 0.4	99	0.61	0.93	23 of 26	GA1550 biotite	98.79 ± 0.96	5.543E-10	28.294 ± 0.036	121.2 ± 0.4 [0.7]	He et al. (2004)
Lower part of formation	L3001	Tuff	$^{40}Ar/^{39}Ar$ plateau	Sanidine & orthoclase	120.1 ± 0.5	58	0.47	0.83	6 of 15	GA1550 biotite	98.79 ± 0.96	5.543E-10	28.294 ± 0.036	121.2 ± 0.5 [0.8]	He et al. (2004)
							0	1.00	2 of 2 samples				Weighted mean	**121.2 ± 0.3 [0.6]**	
Immediately above Yixian Fm.	JFT07-1	Tuff	$^{40}Ar/^{39}Ar$ single crystal total fusion	Sanidine	122.6 ± 0.4	-	0.83	0.64	16 of 16	FC sanidine	28.02 ± 0.28	5.543E-10	28.294 ± 0.036	123.8 ± 0.4 [0.7]	Chang et al. (2009)
Immediately above Yixian Fm.	JFT07-1	Tuff	$^{40}Ar/^{39}Ar$ plateau	Sanidine	121.8 ± 0.4	100	0.65	0.80	12 of 12 steps	FC sanidine	28.02 ± 0.28	5.543E-10	28.294 ± 0.036	123.0 ± 0.4 [0.7]	Chang et al. (2009)
Immediately above Yixian Fm.	JFT07-1	Tuff	$^{40}Ar/^{39}Ar$ plateau	Sanidine	122.2 ± 0.4	97	0.75	0.68	10 of 12 steps	FC sanidine	28.02 ± 0.28	5.543E-10	28.294 ± 0.036	123.4 ± 0.4 [0.7]	Chang et al. (2009)
							1.18	0.21	40 of 40				Weighted	**123.4 ± 0.3 [0.6]**	Chang et

									steps			mean		al. (2009)
Jingangshan Member, Yixian Formation														
Upper Jingangshan Member	6	Volcanic breccia	40Ar/39Ar plateau	Plagioclase	121.5 ± 1.8	100	?	>0.05	?	Hb3gr	1079	5.543E-10	1081.0 ± 1.2	121.7 ± 1.8 [2.1]	Smith et al. (1995)
Upper Jingangshan Member	6	Volcanic breccia	40Ar/39Ar plateau	Biotite	121.6 ± 1.0	90	?	>0.05	?	Hb3gr	1079	5.543E-10	1081.0 ± 1.2	121.8 ± 1.0 [1.3]	Smith et al. (1995)
						0.01	0.92	2 of 2 samples					**Weighted mean**	**121.8 ± 0.9 [1.2]**	
Upper Jingangshan Member	5	Dolerite	40Ar/39Ar inverse isochron	Whole-rock	120.9 ± 0.8	73	?	>0.05	?	Hb3gr	1079	5.543E-10	1081.0 ± 1.2	121.1 ± 0.8 [1.1]	Smith et al. (1995)
Upper Jingangshan Member	5	Dolerite	40Ar/39Ar inverse isochron	Whole-rock	120.8 ± 0.8	59	?	>0.05	?	Hb3gr	1079	5.543E-10	1081.0 ± 1.2	121.0 ± 0.8 [1.1]	Smith et al. (1995)
						0.03	0.86	2 of 2 samples					**Weighted mean**	**121.1 ± 0.6 [0.9]**	
Upper Lava Unit, Yixian Formation														
Within M0r (Upper Lava Unit?)	M9	Andesite	40Ar/39Ar plateau	Groundmass	*121.2 ± 1.3*	*45*	*1.05*	0.39	6 of 14	85G003 TCR sanidine	28.34 ± 0.28	5.543E-10	28.608 ± 0.033	-	He et al. (2008)
Within M0r (Upper Lava Unit?)	M14	Andesite	40Ar/39Ar plateau	Groundmass	*120.2 ± 1.5*	*44*	*2.04*	0.07	5 of 9	85G003 TCR sanidine	28.34 ± 0.28	5.543E-10	28.608 ± 0.033	-	He et al. (2008)
Within M0r (Upper Lava Unit?)	ZCZ28	Andesite	40Ar/39Ar plateau	Groundmass	121.7 ± 0.8	89	0.96	0.46	9 of 12	85G003 TCR sanidine	28.34 ± 0.28	5.543E-10	28.608 ± 0.033	**122.9 ± 0.8 [1.1]**	He et al. (2008)
Upper Lava Unit	YL30	Basalt	40Ar/39Ar plateau	Whole-rock	122.1 ± 1.0	97	0.87	0.52	7 of 12	GA1550 biotite	97.9 Ma	5.543E-10	99.738 ± 0.104	**124.4 ± 1.0 [1.3]**	Wang et al. (2001b)
Upper Lava Unit (reverse polarity, M1r?)	Sample A	Basalt?	40Ar/39Ar plateau	Groundmass	123.7 ± 0.9	77	0.2	0.99	7 of 10	-	-	5.543E-10	-	-	Zhu et al. (2007)

Jianshangou Member, Yixian Formation															
Upper Jianshangou Member	LX-HBJ-6	Tuff	U-Pb SHRIMP	Zircon	122.8 ± 1.6	-	0.47	0.89	10 of 10	-	-	-	-	**122.8 ± 1.6 [1.7]**	Yang et al. (2007)
Upper Jianshangou Member	YX07-3	Tuff	⁴⁰Ar/³⁹Ar plateau	Sanidine	122.2 ± 1.8	100	0.89	0.47	4 of 4 steps	FC sanidine	28.02 ± 0.28	5.543E-10	28.294 ± 0.036	123.4 ± 1.8 [2.1]	Chang et al. (2009)
Upper Jianshangou Member	YX07-3	Tuff	⁴⁰Ar/³⁹Ar plateau	Sanidine	122.5 ± 1.7	100	0.02	1.00	4 of 4 steps	FC sanidine	28.02 ± 0.28	5.543E-10	28.294 ± 0.036	123.7 ± 1.7 [2.0]	Chang et al. (2009)
Upper Jianshangou Member	YX07-3	Tuff	⁴⁰Ar/³⁹Ar plateau	Sanidine	123.5 ± 1.4	92	0.8	0.55	5 of 6 steps	FC sanidine	28.02 ± 0.28	5.543E-10	28.294 ± 0.036	124.7 ± 1.4 [1.7]	Chang et al. (2009)
Upper Jianshangou Member	YX07-3	Tuff	⁴⁰Ar/³⁹Ar plateau	Sanidine	122.7 ± 1.1	100	0.58	0.75	6 of 6 steps	FC sanidine	28.02 ± 0.28	5.543E-10	28.294 ± 0.036	123.9 ± 1.1 [1.4]	Chang et al. (2009)
Upper Jianshangou Member	YX07-3	Tuff	⁴⁰Ar/³⁹Ar plateau	Sanidine	122.0 ± 2.0	100	0.75	0.56	4 of 4 steps	FC sanidine	28.02 ± 0.28	5.543E-10	28.294 ± 0.036	123.2 ± 2.0 [2.3]	Chang et al. (2009)
Upper Jianshangou Member	YX07-3	Tuff	⁴⁰Ar/³⁹Ar plateau	Sanidine	123.2 ± 1.6	100	0.11	0.98	4 of 4 steps	FC sanidine	28.02 ± 0.28	5.543E-10	28.294 ± 0.036	124.4 ± 1.6 [1.9]	Chang et al. (2009)
					122.8 ± 0.6	-	0.5	0.99	37 of 38 plateau steps				**Weighted mean**	**124.0 ± 0.6 [0.9]**	
Lower Jianshangou Member	99L-HDZ1	Tuff	*⁴⁰Ar/³⁹Ar single crystal total fusion*	*Sanidine*	*125.0 ± 0.5*	-	?	?	*24 of 24*	*FC sanidine*	*28.02 ± 0.28*	*5.54 E-10*	*28.294 ± 0.036*	*126.2 ± 0.5 [0.8]*	*Swisher et al. (2002)*
Lower Jianshangou Member	P1T-2	Tuff	⁴⁰Ar/³⁹Ar single crystal total fusion	Sanidine	124.6 ± 0.4	-	1	0.47	35 of 35	FC sanidine	28.02 ± 0.28	5.543E-10	28.294 ± 0.036	125.8 ± 0.4 [0.7]	Swisher et al. (1999)

Lower Jianshangou Member	P4T-1	Tuff	^{40}Ar/^{39}Ar single crystal total fusion	Sanidine	124.5 ± 0.5	-	1.05	0.38	33 of 34	FC sanidine	28.02 ± 0.28	5.543E-10	28.294 ± 0.036	125.8 ± 0.5 [0.8]	Swisher et al. (1999)
Lower Jianshangou Member	P4T-1	Tuff	^{40}Ar/^{39}Ar plateau	Sanidine	124.6 ± 0.3	100	1.13	0.29	23 of 24	FC sanidine	28.02 ± 0.28	5.543E-10	28.294 ± 0.036	125.8 ± 0.3 [0.6]	Swisher et al. (1999)
Lower Jianshangou Member	*99L-S1*	*Tuff*	*^{40}Ar/^{39}Ar single crystal total fusion*	*Sanidine*	*125.0 ± 0.4*	*-*	*?*	*?*	*24 of 24*	*FC sanidine*	*28.02 ± 0.28*	*5.54E-10*	*28.294 ± 0.036*	*126.2 ± 0.5 [0.8]*	*Swisher et al. (2002)*
Lower Jianshangou Member	YL31	Tuff	U-Pb TIMS	Zircon	125.2 ± 0.9	-	0.03	1.00	4 of 5	-	-	-	-	125.2 ± 0.9 [1.0]	Wang et al. (2001a)
Lower Jianshangou Member	LX-SHT-12	Tuff	U-Pb SHRIMP	Zircon	124.7 ± 2.7	-	1.4	0.20	8 of 9	-	-	-	-	124.7 ± 2.7 [2.8]	Yang et al. (2007)
Lower Jianshangou Member	YX07-4	Tuff	^{40}Ar/^{39}Ar single crystal total fusion	Sanidine	123.8 ± 0.5	-	0.65	0.84	17 of 17	FC sanidine	28.02 ± 0.28	5.543E-10	28.294 ± 0.036	125.0 ± 0.5 [0.8]	Chang et al. (2009)
Lower Jianshangou Member	YX07-4	Tuff	^{40}Ar/^{39}Ar plateau	Sanidine	124.1 ± 0.4	90	0.63	0.75	8 of 13	FC sanidine	28.02 ± 0.28	5.543E-10	28.294 ± 0.036	125.3 ± 0.4 [0.7]	Chang et al. (2009)
							2.1	0.05	7 of 7 samples				**Weighted mean**	**125.6 ± 0.3 [0.6]**	
Lower Lava Unit, Yixian Formation															
Lower Lava Unit (normal polarity)	Sample B	Basalt?	^{40}Ar/^{39}Ar plateau	Groundmass	126.0 ± 1.0	69	0.55	0.77	6 of 10 steps	-	-	5.543E-10	-	-	Zhu et al. (2007)
Lower Lava Unit	*YL29*	*Basalt*	*^{40}Ar/^{39}Ar plateau*	*Whole-rock*	*128.9 ± 1.5*	*56*	*0.22*	*0.80*	*3 of 15*	*GA1550 biotite*	*97.9 Ma*	*5.54E-10*	*99.738 ± 0.104*	*131.3 ± 1.5 [1.8]*	*Wang et al. (2001b)*
Lower Lava Unit	YX07-2	Basalt	^{40}Ar/^{39}Ar plateau	Groundmass	126.1 ± 0.5	67	1.72	0.13	5 of 17 steps	FC sanidine	28.02 ± 0.28	5.543E-10	28.294 ± 0.036	**127.3 ± 0.5 [0.8]**	Chang et al.

															(2009)
Lower Lava Unit	*YX07-2*	*Basalt*	*$^{40}Ar/^{39}Ar$ plateau*	*Groundmass*	*126.4 ± 0.5*	*49.6*	*0.19*	*0.94*	*4 of 13 steps*	*FC sanidine*	*28.02 ± 0.28*	*5.54E-10*	*28.294 ± 0.036*	*-*	*Chang et al. (2009)*
Lower Lava Unit, immediately above Lujiatun Member	SYNU-005	Basalt	$^{40}Ar/^{39}Ar$ plateau	Groundmass	126.0 ± 0.8	100	0.91	0.53	13 of 13	FC sanidine	28.294 ± 0.036	5.531E-10	28.294 ± 0.036	126.0 ± 0.8 [1.1]	Chang et al. (2017)
Lower Lava Unit, immediately above Lujiatun Member	SYNU-010	Basalt	$^{40}Ar/^{39}Ar$ plateau	Groundmass	125.8 ± 1.0	100	1.4	0.15	13 of 13	FC sanidine	28.294 ± 0.036	5.531E-10	28.294 ± 0.036	125.8 ± 1.0 [1.3]	Chang et al. (2017)
													Weighted mean	**125.9 ± 0.6 [0.9]**	
Lujiatan Member, Yixian Formation															
Lujiatan Member	YX07-6	Tuff	$^{40}Ar/^{39}Ar$ plateau	Groundmass	129.7 ± 0.5	68	0.75	0.63	7 of 14	FC sanidine	28.02 ± 0.28	5.543E-10	28.294 ± 0.036	130.9 ± 0.5 [0.8]	Chang et al. (2009)
Lujiatan Member	LX-HBJ-1	Tuff	U-Pb SHRIMP	Zircon	124.9 ± 1.7	-	0.9	0.51	8 of 10	-	-	-	-	**124.9 ± 1.7 [1.8]**	Yang et al. (2007)
Lujiatan Member	L3003	Tuff	$^{40}Ar/^{39}Ar$ plateau	Sanidine & orthoclase	123.0 ± 1.5	75	1.6	0.13	7 of 14	GA1550 biotite	98.79 ± 0.96	5.543E-10	28.294 ± 0.036	124.2 ± 1.5 [1.8]	He et al. (2006)
Lujiatan Member	L3004	Tuff	$^{40}Ar/^{39}Ar$ plateau	Sanidine & orthoclase	123.3 ± 1.6	78	1.24	0.26	9 of 13	GA1550 biotite	98.79 ± 0.96	5.543E-10	28.294 ± 0.036	124.5 ± 1.6 [1.9]	He et al. (2006)
							0.08	0.78	2 of 2 samples				Weighted mean	**124.3 ± 1.1 [1.4]**	

Table 3: Summary of zircon U-Pb TIMS age data from a lower Aptian bentonite within the Great Valley Group, California, USA (Shimokawa, 2010). U-Pb data recalculated using decay constants of Steiger and Jäger (1977) and $^{238}U/^{235}U$ ratio of 137.82 (Hiess et al., 2012).

Site	Stratigraphic Position	Sample Name	Lithology	Method	Mineral	Age (Ma ± 2σ [inc. decay	MSWD	p	n	Source

						constants])				
Great Valley Group	lower Aptian	MC888	Bentonite	U–Pb TIMS	Zircon	**124.08 ± 0.15 [0.23]**	1.7	0.16	4 of 7 spots	Shimokawa (2010)

Table 4: Summary of $^{40}Ar/^{39}Ar$ results for the Greater Ontong Java Event, including ages from the Ontong Java (Chambers et al., 2004; Mahoney et al., 1993; Tejada et al., 1996; Tejada et al., 2002), Manihiki (Hoernle et al., 2010; Ingle et al., 2007) and Hikurangi Plateaus (Hoernle et al., 2010; Timm et al., 2011). Bold ages indicate reliable age constraints. Ages recalculated using decay constants and intercalibration ratios of Renne et al. (2011) and Baksi et al. (1996), respectively.

Stratigraphic Position	Sample Name	Lithology	Method	Mineral	Original Age (Ma ± 2σ)	^{39}Ar in plateau	MSWD	p	n	Standard	Original standard age (Ma ± 1σ)	Original Decay Constant ($\lambda_\epsilon+\lambda_\beta$)	New standard age (Ma ± 2σ)	Recalculated age (Ma ± 2σ [inc. decay constants])	Source
Ontong Java Plateau															
ODP Site 807	75R-2, 129-131	Basalt	$^{40}Ar/^{39}Ar$ plateau	Whole-rock	121.0 ± 9.0	80	?	?		85G003 TCR sanidine	27.92 ± 0.04	5.54E-10	28.608 ± 0.033	**123.9 ± 9.2 [9.5]**	Mahoney et al. (1993)
ODP Site 807	78R-1, 67-69	Basalt	$^{40}Ar/^{39}Ar$ plateau	Whole-rock	121.4 ± 3.8	75	?	?		85G003 TCR sanidine	27.92 ± 0.04	5.54E-10	28.608 ± 0.033	**124.3 ± 3.9 [4.2]**	Mahoney et al. (1993)
ODP Site 807	80R-11 52-55	Basalt	$^{40}Ar/^{39}Ar$ plateau	Whole-rock	119.9 ± 5.2	100	?	?		85G003 TCR sanidine	27.92 ± 0.04	5.54E-10	28.608 ± 0.033	**122.8 ± 5.3 [5.6]**	Mahoney et al. (1993)
ODP Site 807	84R-6, 0-3	Basalt	$^{40}Ar/^{39}Ar$ plateau	Whole-rock	123.4 ± 5.0	97	?	>0.05	5 of 6 steps	85G003 TCR sanidine	27.92 ± 0.04	5.54E-10	28.608 ± 0.033	**126.4 ± 5.1 [5.4]**	Mahoney et al. (1993)
ODP Site 807	90R-1, 38-41	Basalt	$^{40}Ar/^{39}Ar$ plateau	Whole-rock	124.7 ± 4.4	100	?	?		85G003 TCR sanidine	27.92 ± 0.04	5.54E-10	28.608 ± 0.033	**127.7 ± 4.5 [4.8]**	Mahoney et al. (1993)
ODP Site 807	93R-31 15-18	Basalt	$^{40}Ar/^{39}Ar$ plateau	Whole-rock	122.1 ± 4.4	68	?	?		85G003 TCR sanidine	27.92 ± 0.04	5.54E-10	28.608 ± 0.033	**125.0 ± 4.5 [4.8]**	Mahoney et al. (1993)
DSDP Site 289	132-4,79-81	Basalt	$^{40}Ar/^{39}Ar$ plateau	Whole-rock	121.7 ± 5.4	100	?	?		85G003 TCR sanidine	27.92 ± 0.04	5.54E-10	28.608 ± 0.033	124.6 ± 5.5 [5.8]	Mahoney et al. (1993)

Location	Sample	Rock	Method	Material	Age	%			Steps	Standard		Decay		Age	Reference
DSDP Site 289	132-4, 122-125	Basalt	^{40}Ar/^{39}Ar plateau	Whole-rock	122.8 ± 4.8	100	?	>0.05	6 of 6 steps	85G003 TCR sanidine	27.92 ± 0.04	5.54 E-10	28.608 ± 0.033	125.8 ± 4.9 [5.2]	Mahoney et al. (1993)
							0.11	0.74	2 of 2 samples				Weighted mean	125.3 ± 3.6 [3.9]	
ODP Site 1184	*Several from subunit IIE*	*Basaltic clasts*	*^{40}Ar/^{39}Ar single crystal total fusion*	*Plagioclase*	*123.5 ± 3.6*	*61*	*0.20*	*0.94*	*5 of 5*	*FC sanidine*	*28.02 ± 0.28*	*5.54 E-10*	*-*	*-*	*Chambers et al. (2004)*
Malaita Island	KF36	Basalt	^{40}Ar/^{39}Ar plateau	Whole-rock	120.7 ± 3.2	62	?	?	4 steps	FCT-3 biotite	27.55 ± 0.12	5.54 E-10	28.4095 ± 0.003	**124.7 ± 3.3 [3.6]**	Tejada et al. (2002)
Malaita Island	8374	Basalt	^{40}Ar/^{39}Ar plateau	Whole-rock	122.3 ± 4.8	67	?	>0.05	5 steps	85G003 TCR sanidine	27.92 ± 0.04	5.54 E-10	28.608 ± 0.033	**125.2 ± 4.9 [5.2]**	Mahoney et al. (1993)
Malaita Island	P43	Basalt	^{40}Ar/^{39}Ar plateau	Whole-rock	123.3 ± 5.8	79	?	>0.05	5 of 6 steps	85G003 TCR sanidine	27.92 ± 0.04	5.54 E-10	28.608 ± 0.033	**126.3 ± 5.9 [6.2]**	Mahoney et al. (1993)
Malaita Island	SG7	Basalt	^{40}Ar/^{39}Ar plateau	Whole-rock	123.1 ± 2.1	100	?	?	4 steps	FCT-3 biotite	27.55 ± 0.12	5.54 E-10	28.4095 ± 0.003	**127.2 ± 2.2 [2.5]**	Tejada et al. (2002)
Malaita Island	ML475	Basalt	^{40}Ar/^{39}Ar plateau	Whole-rock	123.2 ± 3.0	90	?	?	5 steps	FCT-3 biotite	27.55 ± 0.12	5.54 E-10	28.4095 ± 0.003	**127.3 ± 3.1 [3.4]**	Tejada et al. (2002)
Malaita Island	KF53	Basalt	^{40}Ar/^{39}Ar plateau	Whole-rock	124.9 ± 3.8	59	?	?	5 steps	FCT-3 biotite	27.55 ± 0.12	5.54 E-10	28.4095 ± 0.003	**129.1 ± 3.9 [4.2]**	Tejada et al. (2002)
Malaita Island	*SGB10*	*Basalt*	*^{40}Ar/^{39}Ar plateau*	*Whole-rock*	*128.2 ± 8.5*	*44*	*?*	*?*	*5 steps*	*FCT-3 biotite*	*27.55 ± 0.12*	*5.54 E-10*	*28.4095 ± 0.003*	*-*	*Tejada et al. (2002)*
Santa Isabel Island		Basalt	^{40}Ar/^{39}Ar plateau	Whole-rock	122.9 ± 3.0	100	?	>0.05	4 steps	FCT-3 biotite	27.7 ± 012	5.54 E-10	28.4095 ± 0.003	**126.3 ± 3.1 [3.4]**	Tejada et al. (1996)
Ramos Island	I221	Basalt	^{40}Ar/^{39}Ar plateau	Whole-rock	119.6 ± 3.2	100	?	>0.05	4 steps	FCT-3 biotite	27.7 ± 0.2	5.54 E-10	28.4095 ± 0.003	**123.0 ± 3.3 [3.6]**	Tejada et al. (1996)
Manihiki Plateau															
DSDP 317, Manihiki Plateau	32R2, 54-62 cm	Basalt	^{40}Ar/^{39}Ar plateau	Plagioclase	117.0 ± 4.7	93	0.64	0.81	13 of 20	TCR-2 sanidine	27.87 ± 0.04	5.54 E-10	28.608 ± 0.033	120.0 ± 4.8 [5.1]	Hoernle et al. (2010)

Location	Sample	Rock	Method	Material	Age	%	MSWD	P	steps	Standard	Age std	λ		Age	Reference
DSDP 317, Manihiki Plateau	32R2, 54-62 cm	Basalt	$^{40}Ar/^{39}Ar$ plateau	Plagioclase	116.4 ± 6.0	89	1.2	0.27	14 of 20	TCR-2 sanidine	27.87 ± 0.04	5.54E-10	28.608 ± 0.033	119.4 ± 6.2 [6.5]	Hoernle et al. (2010)
					116.7 ± 3.7		1.19		30 of 40 steps				**Weighted mean**	**119.7 ± 3.8 [4.1]**	
DSDP 317, Manihiki Plateau	34R4, 125-135 cm	Basalt	$^{40}Ar/^{39}Ar$ plateau	Plagioclase	117.3 ± 8.0	100	0.98	0.48	19 of 19	TCR-2 sanidine	27.87 ± 0.04	5.54E-10	28.608 ± 0.033	120.3 ± 8.0 [8.3]	Hoernle et al. (2010)
DSDP 317, Manihiki Plateau	34R4, 125-135 cm	Basalt	$^{40}Ar/^{39}Ar$ plateau	Plagioclase	115.8 ± 6.7	100	1.3	0.18	20 of 20	TCR-2 sanidine	27.87 ± 0.04	5.54E-10	28.608 ± 0.033	118.8 ± 6.7 [7.0]	Hoernle et al. (2010)
					116.4 ± 5.1		1.1	0.29	39 of 39 steps				**Weighted mean**	**119.4 ± 5.2 [5.5]**	
Manihiki Plateau	SO 193 DR 52-2	Basalt	$^{40}Ar/^{39}Ar$ plateau	Glass	124.2 ± 0.9	70	1.02	0.42	10 of 23	FCT-3 biotite	28.030 ± 0.003	5.3E-10	28.495 ± 0.003	126.1 ± 0.9 [1.2]	Timm et al. (2011)
Manihiki Plateau	SO 193 DR 52-2	Basalt	$^{40}Ar/^{39}Ar$ plateau	Glass	123.7 ± 0.9	81	0.93	0.50	11 of 16	FCT-3 biotite	28.030 ± 0.003	5.3E-10	28.495 ± 0.003	125.6 ± 0.9 [1.2]	Timm et al. (2011)
					124.0 ± 0.6		1.00	0.46	21 of 39 steps				**Weighted mean**	**125.9 ± 0.6 [0.9]**	
Manihiki Plateau	SO 193 DR 18-4B	Basalt	$^{40}Ar/^{39}Ar$ plateau	Plagioclase	125.2 ± 8.3	92.3	1.6	0.39	17 of 19	TCR-2 sanidine	27.87 ± 0.04	5.54E-10	28.608 ± 0.033	128.4 ± 8.3 [8.6]	Timm et al. (2011)
Manihiki Plateau	SO 193 DR 46-1	Basalt	$^{40}Ar/^{39}Ar$ plateau	Plagioclase	125.0 ± 2.1	58.9	2.1	0.05	7 of 18	TCR-2 sanidine	27.87 ± 0.04	5.54E-10	28.608 ± 0.033	128.2 ± 2.1 [2.4]	Timm et al. (2011)
Manihiki Plateau	SO 193 DR 26-1	Basalt	$^{40}Ar/^{39}Ar$ plateau	Glass	124.5 ± 1.5	90.2	1.5	0.10	15 of 20	TCR-2 sanidine	27.87 ± 0.04	5.54E-10	28.608 ± 0.033	127.7 ± 1.5 [1.8]	Timm et al. (2011)
Manihiki Plateau	SO 193 DR 26-7	Basalt	$^{40}Ar/^{39}Ar$ plateau	Glass	122.9 ± 1.6	80.3	0.57	0.84	11 of 20	TCR-2 sanidine	27.87 ± 0.04	5.54E-10	28.608 ± 0.033	126.0 ± 1.6 [1.9]	Timm et al. (2011)
Manihiki Plateau	Dr2-1	Basalt	$^{40}Ar/^{39}Ar$ plateau	Groundmass	117.9 ± 3.5	83	0.028	1.00	5 of 7	EB-1 biotite	91.4 ± 0.5	5.54E-10	-	-	Ingle et al. (2007)
Hikurangi Plateau															

Hikurangi Plateau	*SO168-34-4*	*Basalt*	*40Ar/39Ar single crystal total fusion*	*Plagioclase*	*118.4 ± 4.0*	-	*1.18*	*0.28*	*16 of 16 analyses*	*TCR-2 sanidine*	*27.87 ± 0.04*	*5.53 E-10*	-	-	*Hoernle et al. (2010)*

Table 5: Summary of U-Pb and $^{40}Ar/^{39}Ar$ radioisotopic results for the early emplacement period of the High Arctic large igneous province from depositional sequences (Corfu et al., 2013; Midtkandal et al., 2016; Shipilov and Karyakin, 2011) and intrusions (Corfu et al., 2013; Estrada and Henjes-Kunst, 2013; Evenchick et al., 2015; Polteau et al., 2016; Villeneuve and Williamson, 2006). Bold ages indicate reliable age constraints. U-Pb data recalculated using decay constants of Steiger and Jäger (1977) and $^{238}U/^{235}U$ ratio of 137.82 (Hiess et al., 2012). $^{40}Ar/^{39}Ar$ data recalculated using decay constants and intercalibration ratios of Renne et al. (2011).

Stratigraphic Position	Sample Name	Lithology	Method	Mineral	Original Age (Ma ± 2σ)	^{39}Ar in plateau	MSWD	p	n	Standard	Original standard age (Ma ± 1σ)	Original Decay Constant ($λ_ε + λ_ β$)	New standard age (Ma ± 2σ)	Recalculated age (Ma ± 2σ)	Source
Svalbard															
Barremian Helvetiafjellet Formation, ~40m above OAE1a	DH3, DH7	Bentonite	U–Pb TIMS	Zircon	123.39 ± 0.28	-	1.5	0.12	13 of 21 spots	-	-	-	-	**123.39 ± 0.28 [0.36]**	Corfu et al. (2013); Midtkandal et al. (2016)
Linnevatnet Sill	7A	Mafic sill	U–Pb TIMS	Zircon & Rutile	124.6 ± 0.6	-	1.7	0.17	4 of 9 analyses	-	-	-	-	**124.6 ± 0.6 [0.7]**	Corfu et al. (2013)
Diabasodden	1AX	Pegmatitic portion of mafic sill	U–Pb TIMS	Zircon	124.5 ± 0.6	-	2.4	0.007	4 of 4 spots	-	-	-	-	**124.5 ± 0.6 [0.7]**	Corfu et al. (2013)

Diabasodden	4A	Dolerite sill	$^{40}Ar/^{39}Ar$ plateau	Plagioclase	120.2 ± 1.9	74	0.87	0.52	7 of 14 steps	Taylor Creek Rhyolite	28.619 ± 0.034	5.549E-10	28.608 ± 0.033	**120.2 ± 1.9 [2.2]**	Polteau et al. (2016)
Franz Josef Land															
Dyke, Hayes (Heiss) Island	40-1	Basalt	$^{40}Ar/^{39}Ar$ plateau	Plagioclase	125.2 ± 5.5	?	?	?	?	?	?	?	?	-	Shipilov and Karyakin (2011)
Sill, Hayes (Heiss) Island	80-3	Basalt	$^{40}Ar/^{39}Ar$ plateau	Plagioclase	125.9 ± 2.8	?	?	?	?	?	?	?	?	-	Shipilov and Karyakin (2011)
Severnaya borehole	1893	Mafic sill	U–Pb TIMS	Baddeleyite	121.5 ± 0.3 (min. age)	-	0.85	0.43	3 of 4 spots	-				**min. 121.5 ± 0.3 [0.4]**	Corfu et al. (2013)
Severnaya + Nagursakaya boreholes	2944	Mafic sill	U–Pb TIMS	Zircon	122.2 ± 1.1	-	-	-	1 of 2 spots	-	-	-	-	-	Corfu et al. (2013)
Severnaya borehole	1902 + 1895	Mafic sill	U–Pb TIMS	Zircon	122.7 ± 2.5	-	1.3	0.26	2 of 10 spots	-	-	-	-	-	Corfu et al. (2013)
Sverdrup Basin, Northeastern Canada															
Lightfoot River, Axel Heiberg Island	AX85-037	Dyke	$^{40}Ar/^{39}Ar$ plateau	Whole-rock	128.2 ± 2.1	90	0.49	0.74	5 of 6 steps	FC sanidine	28.03 ± 0.28	5.543E-10	28.294 ± 0.036	**129.4 ± 2.2 [2.5]**	Villeneuve and Williamson (2006)
Haakon Dome Gabbro, Ellef Ringnes Island	10EP001B01	Gabbro	U–Pb TIMS	Zircon	126.6 ± 1.2		1.15	0.33	8 of 23 analyses	-	-	-	-	**126.6 ± 1.2 [1.3]**	Evenchick et al. (2015)
Gabbro Peninsula, Ellef Ringnes Island	11EP062A01	Dolerite	U–Pb TIMS	Baddeleyite	120.8 ± 3.6	-	1.5	0.22	2 of 2 analyses	-	-	-	-	**120.8 ± 3.6 [3.7]**	Evenchick et al. (2015)
Dykes in Pearya Metaseds, Ellesmere Island	SE 158/01	Dolerite	$^{40}Ar/^{39}Ar$ plateau	Whole-rock	122.0 ± 2.4	99	1.03	0.4	9 of 10 steps	LP-6 biotite	128.1	5.54E-10	-	-	Estrada and Henjes-Kunst (2013)

Figure captions

Fig. 1: Global plate reconstruction at 125 Ma using the GPlates model of Young et al. (2018), annotated for sites (locations approximate only) that have been reliably dated in the upper Barremian or lower Aptian via U-Pb or ^{40}Ar/^{39}Ar geochronology.

Fig. 2: MIT Guyot, western Pacific Ocean. (a) Location of the MIT Guyot and ODP site 878 drill hole. (b) Stratigraphic sequence at the MIT Guyot, with biostratigraphic information (Erba et al., 1995; Premoli Silva et al., 1995), magnetic polarity scale (Gee and Nakanishi, 1995) and age data (Pringle and Duncan, 1995). Age data has been recalculated to decay constants and intercalibration ratios of Renne et al. (2011). *C. litt.* = *Chiastozygus litterarius*. HAU. = Hauterivian. (c) Weighted mean ^{40}Ar/^{39}Ar age of upper lava flows (hawaiite).

Fig. 3: Yixian Formation, Liaoning Province, China. (a) Map of the Liaoning Province with sampling sites, modified from Wang et al. (1989) and Wang et al. (2016b). (b) Simplified stratigraphic sequence, modified from Wang et al. (2016a) and Chang et al. (2017). References: 1–(He et al., 2004), 2–(Chang et al., 2009), 3–(Smith et al., 1995), 4–(He et al., 2008), 5–(Wang et al., 2001b), 6–(Yang et al., 2007), 7–(Swisher et al., 1999), 8–(Wang et al., 2001a), 9–(Chang et al., 2017), 10–(He et al., 2006). (c) ^{40}Ar/^{39}Ar apparent age versus the cumulative percentage of ^{39}Ar released for sample ZCZ28 from chron M0r.

Fig. 4: Great Valley Group, California, USA. (a) Generalized stratigraphy of northwestern California, modified from Ernst et al. (2008) and showing sampling site (red star) of Shimokawa (2010). (b) Stratigraphic sequence, showing approximate location of lower Aptian sample MC888, modified from Shimokawa (2010). Calcareous nannofossil zonation from Bralower (1990) and Bralower et al. (1995), with updated biostratigraphy from Bown et al. (1998). (c) U-Pb concordia for lower Aptian sample MC888. Inset: weighted mean of youngest cluster of ^{206}Pb/^{238}U dates.

Fig. 5: Greater Ontong Java Event, southwestern Pacific Ocean. (a) Locations of Ontong Java, Manihiki and Hikurangi Plateaus, with sampling sites and recalculated ages annotated. (b) Stratigraphic sequence of DSDP site 289, annotated with basalt ages (Mahoney et al., 1993), magnetostratigraphy (Hammond et al., 1975), nannofossil zonation (Michael, 1975) and planktonic foraminifera (Sikora and Bergen, 2004). (c) Stratigraphic sequence of ODP site 807, annotated with basalt ages (Mahoney et al., 1993), magnetostratigraphy (Musgrave et al., 1993), nannofossil zonation (Mao and Wise, 1993), planktonic foraminifera (Sliter and Leckie, 1993; Channell et al., 1995) and radiolaria (Takahashi and Ling, 1993). (d) Stratigraphic sequence of DSDP site 317, annotated with basalt ages (Hoernle et al., 2010), magnetostratigraphy (Cockerham and Jarrard, 1976) and planktonic foraminifera (McNulty, 1976). ALB. = Albian, CAM. = Campanian, CEN. = Cenomanian.

Fig. 6: Pre-120 Ma components of the High Arctic large igneous province. (a) Locations of reliably-dated sites in northeastern Canada, Svalbard and Franz Josef Land. (b) Detailed stratigraphic sequence from Longyearbyen core DH1, modified from (Midtkandal et al., 2016). Note that bentonite was not encountered in DH1 and was taken from nearby DH3 and DH7 cores (Corfu et al., 2013; Midtkandal et al., 2016). (c) U-Pb concordia for upper Barremian bentonite samples DH3 and DH7 (two analyses >140 Ma not shown for clarity). (d) $^{206}Pb/^{238}U$ weighted mean ages for youngest 13 analyses (yellow).

Fig. 7: Summary of age constraints for the Barremian–Aptian boundary and the base of chron M0r, with all sources of errors included (including decay constants). Up and down arrows indicate that ages are minima and maxima only, respectively (see text for explanation). Flat bar on Yixian Formation sample indicates it can be no more than 0.59 Myr older 122.9 ± 0.8 Ma. For references to individual ages, refer to Figs. 2–6 and Tables 1–5.
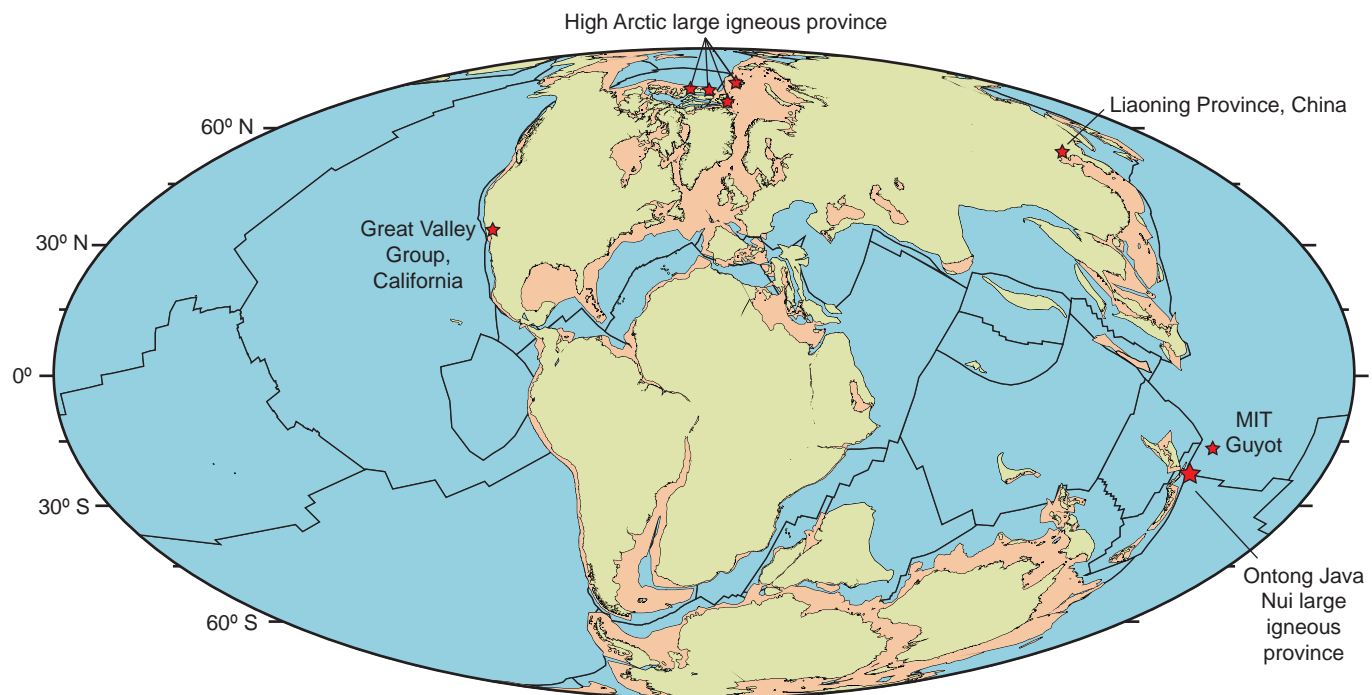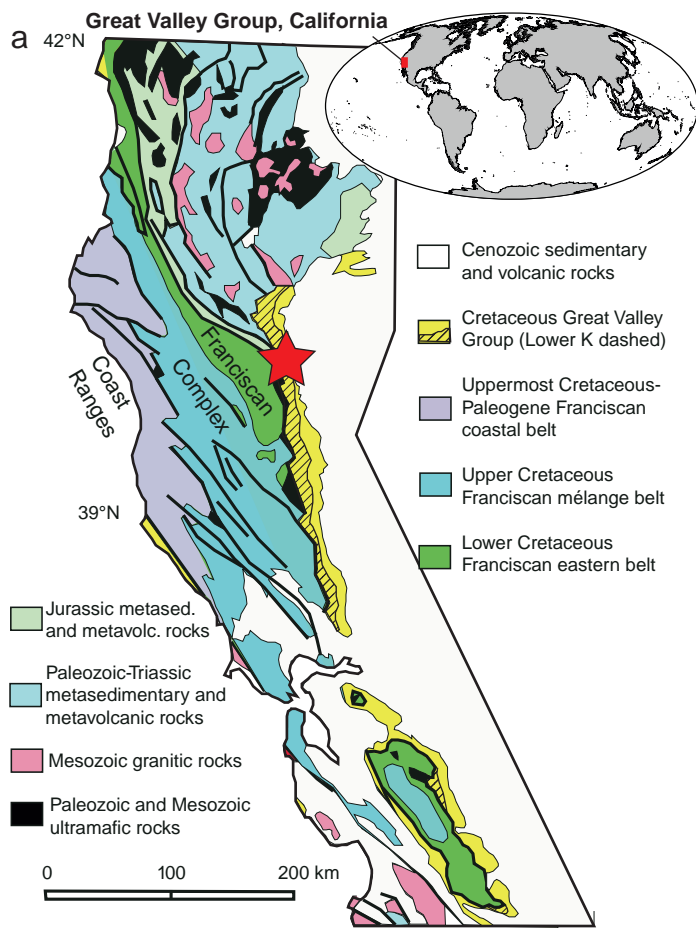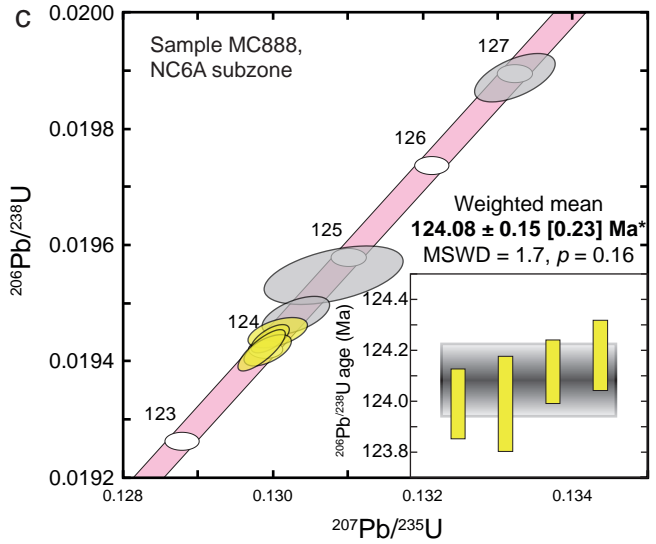
Olierook, Figure 1
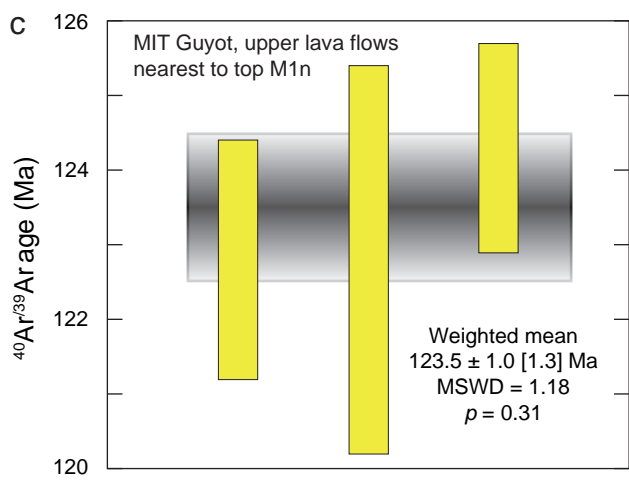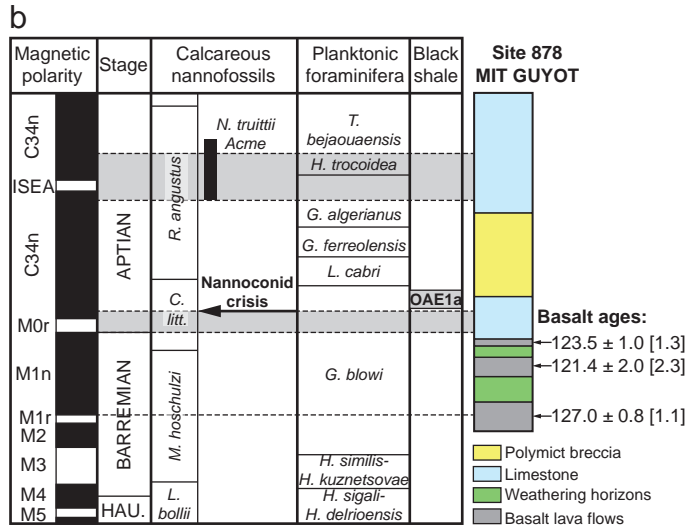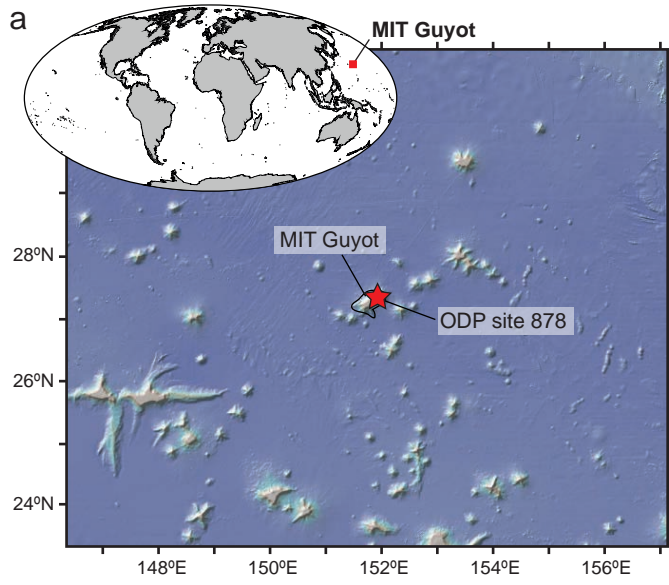
Olierook, Figure 2
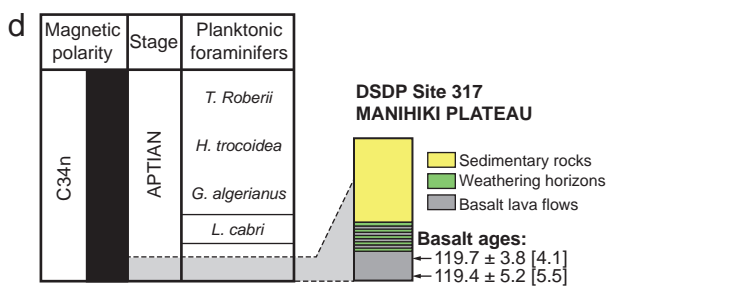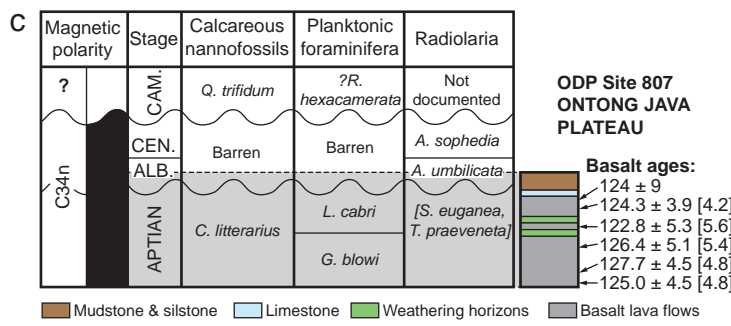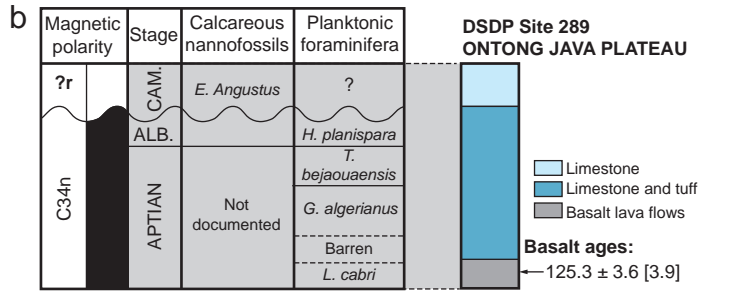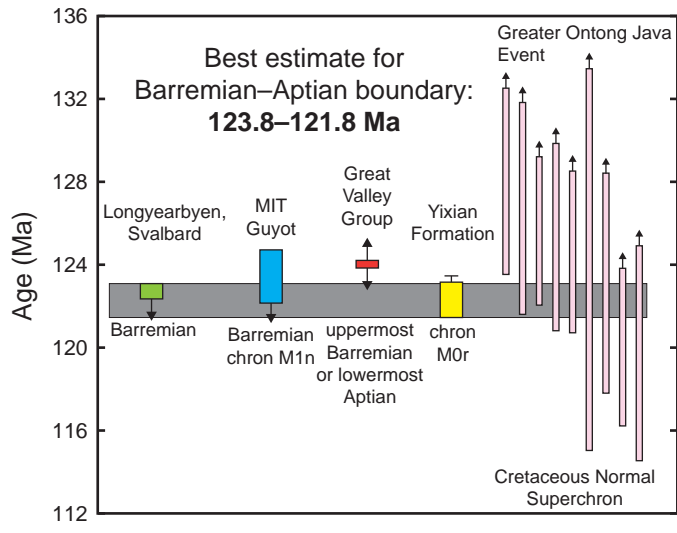
Olierook et al., Figure 3

Olierook et al., Figure 4

Olierook et al., Figure 5
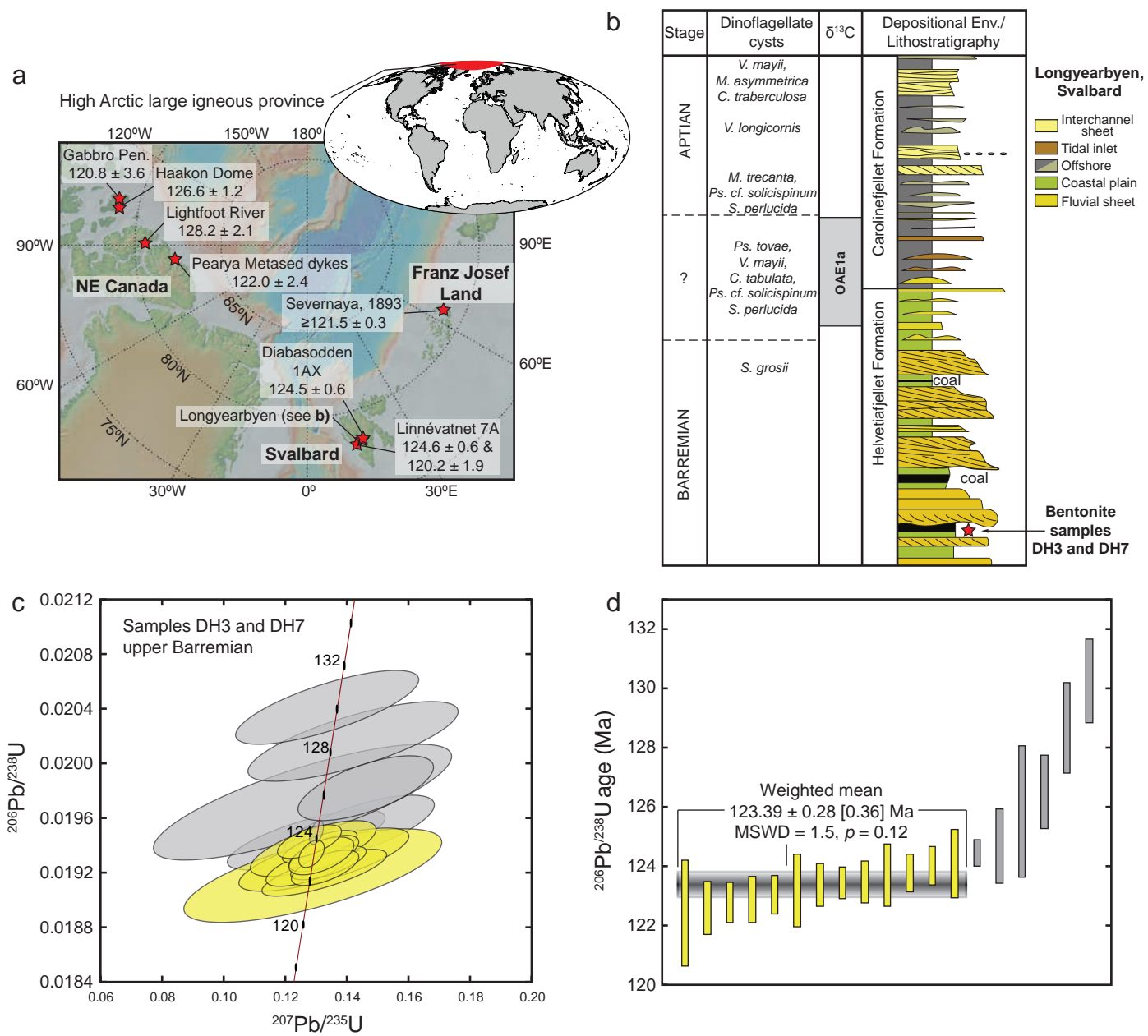
Olierook et al., Figure 6

Olierook et al., Figure 7